Regulation of ABCG2 Through Interactions with Alpha-1-Acid Glycoprotein and EMMPRIN

Sakura Likar

Thesis submitted to the University of Nottingham for

the degree of Master of Research

Abstract

The human ABCG2 transporter, a member of the ATP-binding cassette (ABC) transporter superfamily, plays a crucial role in the efflux of various substrates, including chemotherapeutic drugs from cells. Its involvement in drug efflux has been extensively associated with multidrug resistance (MDR) in cancer cells, highlighting the pressing need for a deeper understanding of ABCG2 regulation. One way that proteins are regulated is through interactions with other proteins, impacting their function. The thesis investigated the possible role of alpha-1-acid glycoprotein (AAG) as an extracellular acceptor of ABCG2 substrates, therefore accelerating efflux. Secondly, the thesis studied whether extracellular matrix metalloproteinase inducer (EMMPRIN) acts to stabilize ABCG2 and increase its expression or stability. ABCG2:AAG interactions were investigated through functional time-course transport assays using stably transfected HEK293T-sfGFP-ABCG2 cells and rates of efflux were measured and compared. Semiquantitative analysis of HEK293T-sfGFP-ABCG2 cells co-transfected with EMMPRIN were studied for ABCG2:EMMPRIN interactions. Addition of AAG was not found to have increased the rate of mitoxantrone efflux by ABCG2. Co-expression with EMMPRIN did not result in increased ABCG2 expression in whole cell lysates. Though results from experiments were inconclusive in relation to the proposed hypotheses, groundwork has been laid out for future protein

biophysical work that enables investigation of ABCG2 protein-protein interactions.

Acknowledgements

This section cannot do justice to the overwhelming gratitude I have for everyone that has supported me throughout this project and thesis. Firstly, I must thank Dr. Ian Kerr, my primary supervisor, for all the support he has provided me during this whirlwind of a year. I knew from the moment we had our first meeting on Microsoft Teams that Ian was going to be the perfect supervisor for my MRes. Moving to a new city, let alone a new country, is hard enough, on top of handling the responsibilities I was going to have as a research masters student. But Ian's warm welcome, along with everyone else in the lab, helped me acclimate to my new home. Ian and Deb made me enjoy my past year doing research here at the university so much that I decided I wanted to stay and do a PhD!

Speaking of Deb Briggs, I appreciate all the help and time she gave me for this project. From the times I "demanded" more DNA for transfections to my ambition to grow as many suspension cultures as humanely possible in our modest lab, Deb was always willing to help and find resources that I needed. If there was an award for "best lab technician," it would certainly have to be handed out to Deb.

Along with Ian and Deb, I need to thank everyone else that is part of the Kerr Lab and Co. This year wouldn't have been as enjoyable if it weren't for the friendships I formed with Norah Alsaigh, Manon Jones, Imogen Rayer, and Susie Entwistle. During frustrating times and the writing process, conversations with you all helped with morale and

renewed motivation. Who knows, it may have rather been the nice cakes or other sweet treats we were having that helped instead. I would also like to thank Dilraj Dhamrait for his part in transfections that needed to be carried out for this project.

Next, I would like to thank Dr. Dave Scott, my secondary supervisor, for his support on this project. I especially appreciate him helping me establish contact with the Membrane Protein Lab (MPL) at Diamond Light Source Ltd for my protein purification work. I really enjoyed our long drive back from the MPL where I believe we (or “I” I should say) talked nonstop about a variety of topics.

At MPL, I would like to thank Dr. Andrew Quigley and Dr. Harish Cheruvara for their advice and expertise in membrane protein purification. Despite low outcomes, they were patient with me while we tried figuring out the best protein purification process.

Finally, I would like to thank my parents who have supported me throughout this MRes journey from afar back in Alaska. In particular, I would like to thank my mom for investing into my education at a young age, understanding its importance for my future. The saying “a mother knows best” is true because she has been insisting from my undergraduate days that I was a good fit for the research life (I didn’t believe her). Perhaps in another life you would be in my position today.

Declaration

This thesis, “Regulation of ABCG2 through interactions with alpha-1-acid glycoprotein and EMMPRIN”, is the result of my own work undertaken during my period of registration at the University of Nottingham under the supervision of Dr. Ian Kerr and Dr. Dave Scott. Technical assistance, and collaborations where relevant, has been acknowledged.

Sakura Likar

Student ID: 20567558

November 2024

Abbreviations

AAG	Alpha-1-acid glycoprotein
ABC	ATP-binding cassette
APS	Ammonium persulfate
ATP	Adenosine triphosphate
BSA	Bovine serum albumin
BSG	Basigin
CMC	Critical micelle concentration
DMEM	Dulbecco's modified eagle medium
DMSO	Dimethyl sulfoxide
DNA	Deoxyribose nucleic acid
ECL	Enhanced chemiluminescence
EDTA	Ethylenediaminetetraacetic acid
EMMPRIN	Extracellular matrix metalloproteinase inducer
FACS	Fluorescence-activated cell sorting
FBS	Foetal bovine serum
FCS	Forward scatter channel
FIDA	Flow-induced dispersion analysis
FSEC	Fluorescence-detection size-exclusion chromatography
HBSS	Hank's balanced salt solution
HEK293S	Human embryonic kidney 293S cell line
HEK293T	Human embryonic kidney 293T cell line
HEPES	4-(2-hydroxyethyl)-1-piperazineethanesulfonic acid
HPLC	High-performance liquid chromatography
HRP	Horseradish peroxidase
MDR	Multidrug resistance
MES	2-(N-Morpholino)ethanesulfonic acid
MIB1	Membrane isolation buffer 1
MIB4	Membrane isolation buffer 4
MMP	Matrix metalloproteinase

MPL	Membrane Protein Lab
MWCO	Molecular weight cut off
MX	Mitoxantrone
nanoDSF	Nano differential scanning fluorimetry
NBD	Nucleotide-binding domain
PBS	Phosphate buffered saline
PBS/Mg^{2+}/Ca^{2+}	Phosphate buffered saline with 1 mM $MgCl_2$ and 0.1 mM $CaCl_2$
PBS/T	Phosphate buffered saline with 0.1% (v/v) Tween-20
PEI	Polyethyleneimine
PFA	Paraformaldehyde
P/S	Penicillin-streptomycin
SD	Standard deviation
SDS-PAGE	Sodium dodecyl sulphate polyacrylamide gel electrophoresis
SEC	Size-exclusion chromatography
SLC	Solute carrier
SMA	Styrene maleic acid
SSC	Side scatter channel
sfGFP	Superfolder green fluorescent protein
TEMED	Tetramethylethylenediamine
TMD	Transmembrane domain
2DG	2-deoxy-D-glucose

Contents

List of Figures

List of Tables

Chapter 1 Introduction

1.1 Membrane Transporters

All living organisms have some form of lipid membrane as an essential protector of their cellular components. It is a dynamic and complex barrier composed of various molecular structures with different morphology and chemical composition that allows vital biochemical reactions to occur. The biological membrane controls the movement of substrates in and out of cells so that important substrates such as nutrients and metabolites can partake in cellular processes while toxic molecules are excluded or exported. Membrane proteins are an integral part of the lipid bilayer and have a multitude of functions including as transporter of molecules, mediators of cell signalling, and anchors for cellular structure (Figure 1.1 A).

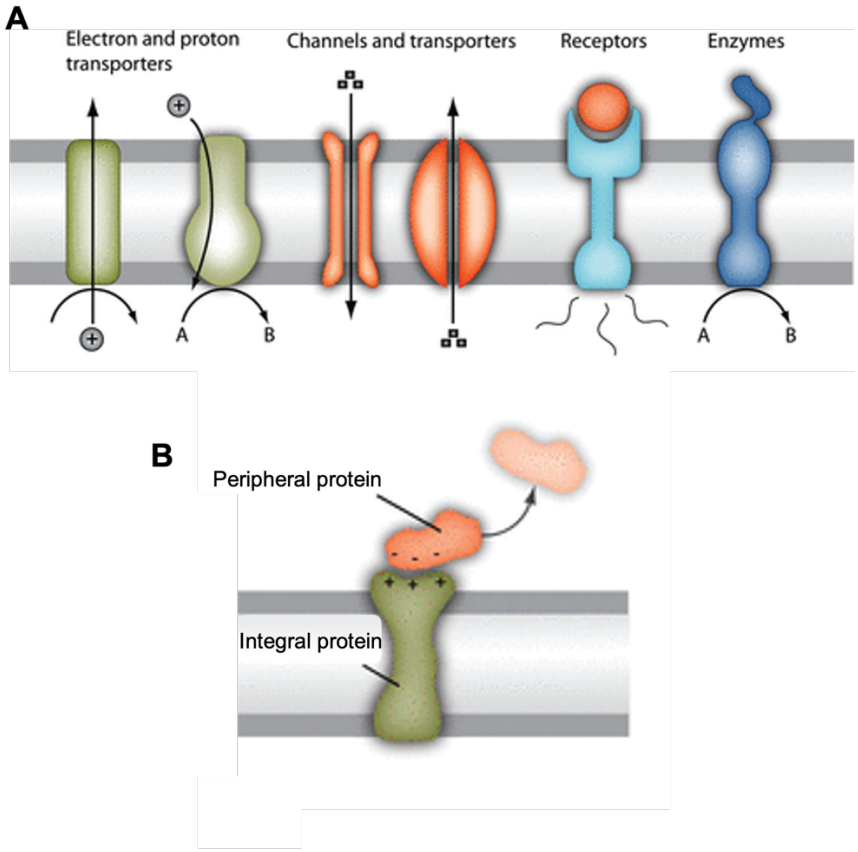

Figure 1.1 – Schematic of the cell membrane. The lipid bilayer (grey) contains a wide range of membrane proteins. These can be transporters, channels, receptors, or enzymes that play key roles in biological processes (**A**). **B** shows how peripheral proteins interact with the lipid bilayer, often interacting with integral proteins embedded within the membrane. Figure adapted from Hedin et al. (2011).

Depending on their interaction with the lipid bilayer, membrane proteins can be broadly categorized as peripheral or integral (Figure 1.1 B; Hedin et al., 2011). Peripheral membrane proteins associate temporarily with the membrane surface through electrostatic and hydrophobic interactions. Meanwhile, integral membrane proteins span the entire bilayer, and all transporter and channel proteins have this integral transmembrane topology. Among humans, two large membrane transporter families are known to comprise most of the transporters vital for everyday cellular functions. These are the solute

carrier (SLC) and ATP-binding cassette (ABC) membrane transporter families. Since this thesis is on the ABCG2 transporter, which is part of the ABC superfamily, focus will be on this group of proteins. For further insight into the SLC transporter family, see Lin et al. (2015).

1.1.1 The ABC Transporter Superfamily

The ABC transporter superfamily is currently the largest known group of transmembrane proteins, categorized into eight subfamilies A through H. They are found in all living species, though the ABCH subfamily is not found in mammals, plants, or fungi (Theodoulou and Kerr, 2015). ABC transporters are generally composed of two nucleotide-binding domains (NBDs) and two transmembrane domains (TMDs). The subfamilies E and F do not have TMDs and thus are not transporters but are still considered part of the ABC family because their NBDs are phylogenetically related to the other subfamilies (Dean and Annilo, 2005). ABC transporters are classified into their subfamilies based on their NBDs, which are highly conserved across various species. Within the NBDs, the Walker A motif binds to adenosine triphosphate (ATP) and works together with the C-loop (also known as the signature motif) and Walker B motif to hydrolyse ATP for energy (Hollenstein et al., 2007). The TMDs, which generally have 6 – 12 membrane-spanning alpha helices (Dean et al., 2022), then use this energy to undergo a conformational change to move substrates across the concentration gradient. TMDs are more variable in their amino acid sequencing and this dictates substrate specificity of the transporters. Two NBDs and two TMDs are required for a functional transporter.

Eukaryotic ABC transporters can be full transporters (with all four domains in one polypeptide) or half transporters (one NBD and one TMD per polypeptide), where half transporters form homodimers or heterodimers (Figure 1.2) to function properly (Dean et al., 2022).

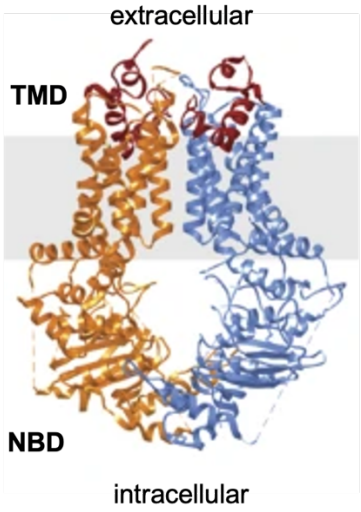

Figure 1.2 – Structure of the G5G8 heterodimer. An example of an ABC heterodimer transporter. ABCG5 (orange) and ABCG8 (blue) come together to form a functional transporter which spans across the lipid bilayer (grey). Figure adapted from Lee et al. (2016).

1.2 ABCG2

1.2.1 Overview as a Human Transporter

ABCG2 is a homodimer transporter that is one of the 48 known human ABC transporters. Along with ABCB1 and ABCC1, it has a key role as a multidrug transporter in many physiological processes due to its broad substrate specificity (Sarkadi et al., 2006). High expression levels of ABCG2 can be found in the epithelial cells of the placenta, small intestines, liver, testes, ovaries, and colon, as well as the endothelial cells of the blood-brain barrier and venules (Doyle and Ross, 2003),

where they function to protect the tissues by excreting and limiting absorption of drugs and xenobiotics (Horsey et al., 2016). During late pregnancy and lactation, ABCG2 is strongly induced in the mammary epithelial tissue and secretes beneficial substrates such as vitamins into milk (van Herwaarden et al., 2007). Contrarily, it also transports toxins into milk (van Herwaarden and Schinkel, 2006). Though its role as a multidrug pump is crucial in keeping toxins out of cells, overexpression of ABCG2 is linked to multidrug resistance (MDR) particularly in cancer cells. Examples of diseases that ABCG2 is found to be overexpressed in are myelocytic leukaemia, breast cancer, thyroid cancer, ovarian cancer, and multiple myeloma (Sajid et al., 2023). With its role in MDR in a variety of cancers, ABCG2 has been an important transporter to study for the improvement of patient outcomes. However, due to its important ability in effluxing a large number of structurally dissimilar substrates (Figure 1.3) to protect cells from toxins, development of therapeutics that target ABCG2 without negative impact on patient's health has been proven to be difficult. Therefore, investigating ABCG2's interactions with other proteins, and in turn observing how these interactions affect ABCG2 regulation is an alternative approach to discover therapeutics to combat ABCG2-conferred MDR.

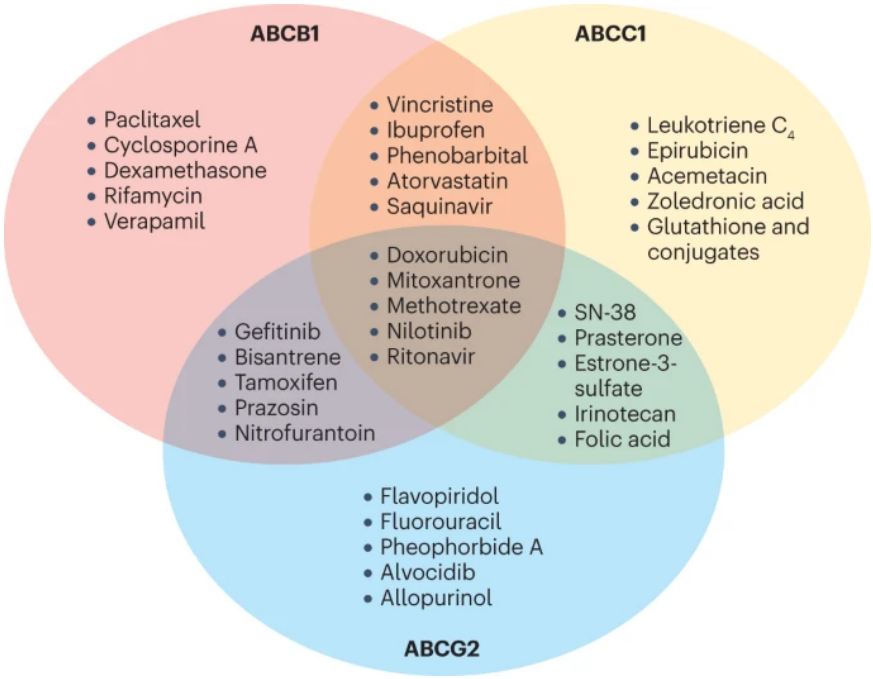

Figure 1.3 – Examples of substrates transported by the three ABC multidrug pumps. ABCB1, ABCC1, and ABCG2 are the three known multidrug pumps in the ABC transporter family. The Venn diagram shows some select substrates that are only transported by one of the multidrug pumps, while overlapping areas shows substrates that can be transported by more than one pump. Figure adapted from Sajid et al. (2023).

1.2.2 Structure and Mechanism

To understand how ABCG2 functions and interacts with other proteins, it is important to understand its structure as a transporter. ABCG2 is considered a half transporter because it is made up of one NBD and one TMD within a single polypeptide chain and must dimerize to be a functional transporter. Higher oligomerization of the protein has been observed, but the physiological significance of these larger assemblies has remained unclear (Wong et al., 2016; Kapoor et al., 2020). Its domains are also considered to be in reverse order compared to most other ABC transporters since the NBD is on the N-terminal end and the TMD, made up of six transmembrane alpha-helices, is on the C-

terminal end (Figure 1.4; Kerr et al., 2011). Even without the presence of bound ATP, the NBDs of the transporter remain in contact (Figure 1.4 A), and these domains are connected to their respective TMD's TM1a through a highly charged linker (Figure 1.4 B; Taylor et al., 2017). The TMD interface is made up of TM2 and TM5a alpha-helices from opposing ABCG2 monomers. Unique to ABCG2 is the long length of the extracellular loop EL3, which connects the TM5c and TM6a together and includes three cysteines (C592, C603, and C608) along with a single N-glycosylation site (N596) (Figure 1.4 B; Taylor et al., 2017). The cysteines C592 and C608 from the same monomer form intramolecular disulfide bonds while the C608 cysteines from opposing monomers form an intermolecular disulfide bond (Figure 1.4 B). The intramolecular disulfide bonds have an important role in stabilizing the EL3 loops, impacting ABCG2 maturation and activity at the plasma membrane (Henriksen et al., 2005; Wakabayashi et al., 2006). Contrarily, the intermolecular disulfide bond seems to not be critical for transport function since mutations destroying the disulfide bond had no impact on drug efflux (Kage et al., 2005). Mutations of N596 prevent glycosylation, causing protein destabilization and enhanced ubiquitin-mediated degradation (Nakagawa et al., 2009).

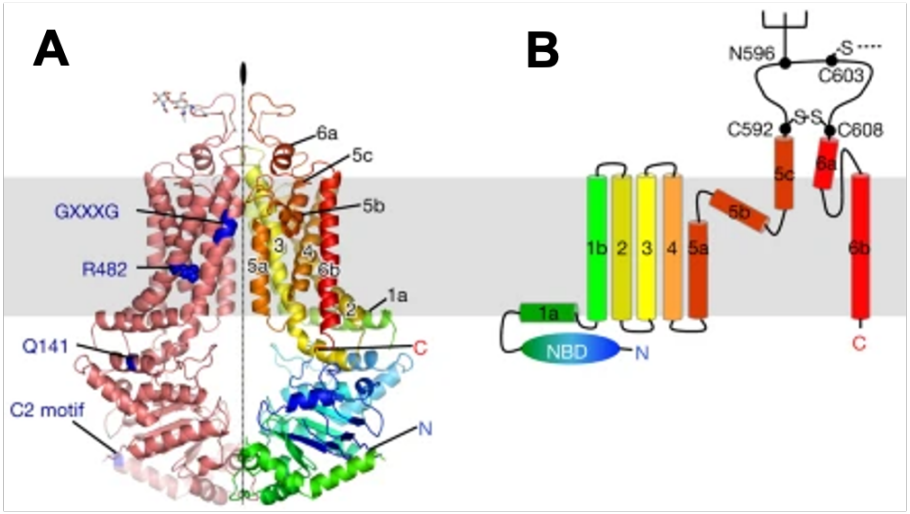

Figure 1.4 – ABCG2 structure and topology. ABCG2 structure is shown in **A**, where the left monomer (salmon) depicts motifs and residues linked with single nucleotide polymorphisms (blue). The right monomer is coloured as a rainbow spectrum and its topology is displayed in **B**. Intramolecular and intermolecular disulfide bonds formed by cysteines (C592, C603, and C608) along with the N-glycosylated residue (N596) are shown. Figure adapted from Taylor et al. (2017).

ABCG2 has a wide range of substrates and inhibitors that it can bind or transport. These include anti-cancer drugs such as mitoxantrone, doxorubicin, and gefitinib (Figure 1.3), and fumitremorgin C-derived inhibitors such as Ko143 (Allen et al., 2002; Kerr et al., 2011). Cavity 1, formed by the two TM2 and TM5a from the monomers, is accessible from the cytosol and spans more than half of the plasma membrane. At the extracellular side is a smaller space, cavity 2, located below the EL3 external loops. The leucine plug, which separates the two cavities, is formed by the L554 residues from both monomers (Taylor et al., 2017; Eckenstaler and Benndorf, 2020). The proposed mechanism is that substrates enter the transporter through cavity 1 and bind to hydrophobic residues nearby the leucine plug (Figure 1.5). ATP binding

then induces a conformation change of the transporter from inward to outward facing, which collapses cavity 1 and forces the substrate to move into cavity 2 (Figure 1.5). The substrate is subsequently released into the extracellular space (Figure 1.5). In the final stage, energy from ATP hydrolysis allows the complex to return to its original conformational state (Figure 1.5; Manolaridis et al., 2018). Both Jackson et al. (2018) and Manolaridis et al. (2018) have demonstrated that Ko143 derivatives also bind to ABCG2 at the cavity 1 site, blocking substrates from accessing the binding site and inhibiting the complex from undergoing the required confirmational changes.

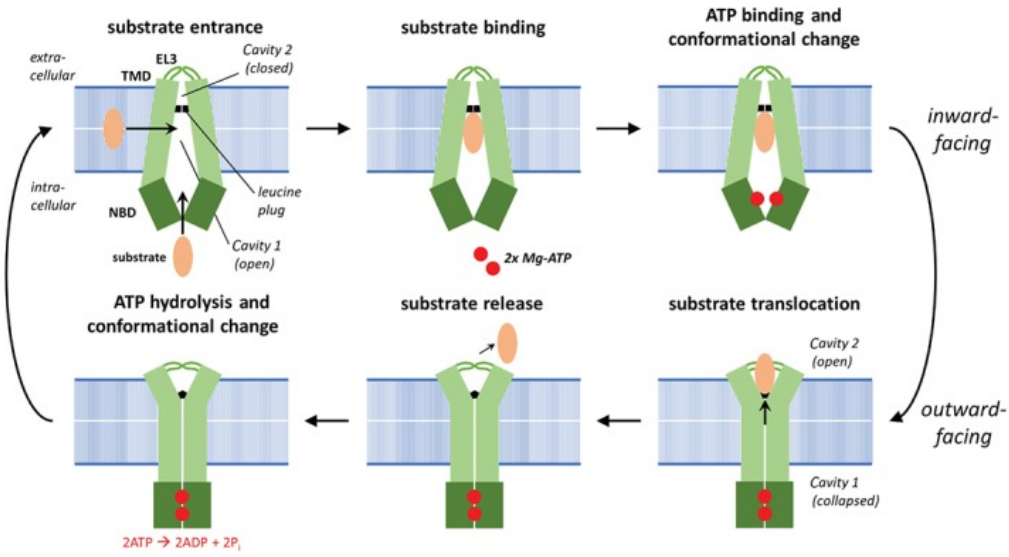

Figure 1.5 – Schematic illustration of the ABCG2 transport cycle. Substrates (peach) enter cavity 1 and then move through the leucine plug and into cavity 2 when ATP (red) is bound to the complex (green). The substrate is then released into the extracellular space and the transporter returns to its original confirmational state through ATP hydrolysis. Figure adapted from Eckenstaler and Benndorf (2020).

1.3 ABCG2's Interaction with Other Proteins

With ABCG2's role in MDR, it is vital to understand ABCG2 protein-protein interactions to develop inhibitors that target these interactions (Arkin et al., 2014) rather than focusing on the drug binding sites with low specificity. One way to determine which proteins ABCG2 interacts with is to use databases such as STRING (Szklarczyk et al., 2023), which complies together known and predicted protein-protein interactions from experimental data and computational work. Figure 1.6 shows the ABCG2 protein-protein interactions complied by STRING. However, the database is not perfect, and Figure 1.6 does not display all the currently known ABCG2 protein-protein interactions. For example, the Pim-1 kinase, not portrayed in Figure 1.6, has been shown to upregulate ABCG2 through phosphorylation, promoting MDR in prostate and pancreatic cancer cells (Xie et al., 2008; Xu et al., 2016). Another unshown protein-protein example is how ABCG2 can regulate metabolism in cancer cells through regulation of SLC1A5, a glutamine transporter (Shi et al., 2024). This leads to an increase in glutaminolysis and enhanced redox regulation. Although these databases are a useful starting point to determine which ABCG2 protein-protein interactions to study, experimental work is just as valuable to prove that these interactions are valid and to discover new protein-protein interactions.

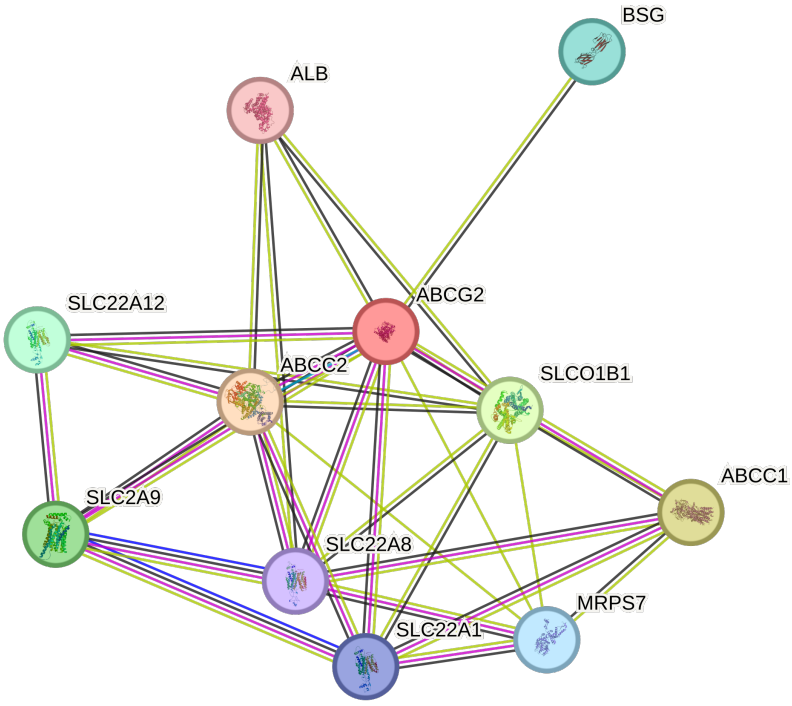

Figure 1.6 – Map of some known and predicted ABCG2 protein-protein interactions. Known interactions that were experimentally determined (magenta lines) or from curated databases (turquoise line) are shown, along with predicted interactions determined from gene co-occurrences (blue). Interactions determined through text mining (green), and co-expression (black) are displayed as well. With reference to Section 1.3.2, BSG is synonymous with EMMPRIN. Image retrieved from STRING.

1.3.1 Alpha-1-acid Glycoprotein; a Possible ABCG2 Interacting Protein

One of the known proteins ABCG2 interacts with is albumin, the most abundant plasma protein in the human circulatory system that functions as a soluble transporter (Fanali et al., 2012). As a major porphyrin transporter, ABCG2 has been shown to bind to haem precursors at the extracellular loop EL3 where substrates are believed to be transferred over to albumin (Desuzinges-Mandon et al., 2010). Furthermore, it has been shown that ABCG2 efflux increased in the presence of both

complete foetal bovine serum (FBS) and pure albumin (Szafraniec and Fiedor, 2021). This interaction is thought to increase ABCG2 efflux by preventing hydrophobic substrates from immediately re-entering cells and thus playing a role in MDR as it causes low bioavailability of drugs.

Like albumin, alpha-1-acid glycoprotein (AAG) is a plasma protein involved in drug transport in the circulatory system. Although ABCG2 interactions with AAG have not been directly studied, the idea is that AAG may also increase ABCG2 efflux in a similar manner to albumin. Research by Park et al. (2021) investigated the effect of ABCG2 single nucleotide polymorphisms on imatinib pharmacokinetics in the presence of AAG. Imatinib, a chemotherapeutic, is a substrate of ABCG2 and binds to AAG. The study found that ABCG2 polymorphisms did not independently affect imatinib pharmacokinetics but significantly influenced it when low AAG levels were present (Park et al. 2021). This suggests a possible ABCG2:AAG interaction during the study.

Building on these findings, as well as previous work on ABCG2:albumin interactions, the first question arose: does AAG interact with ABCG2, and if so, does it enhance ABCG2 efflux (Figure 1.7)? For reasons related to intellectual ownership, ABCG2:albumin interactions were not studied alongside ABCG2:AAG interactions (personal communication Dr. Ian Kerr). However, with the past findings of ABCG2:albumin interactions and the observations by Park et al. (2021), this question became the focus of further investigation.

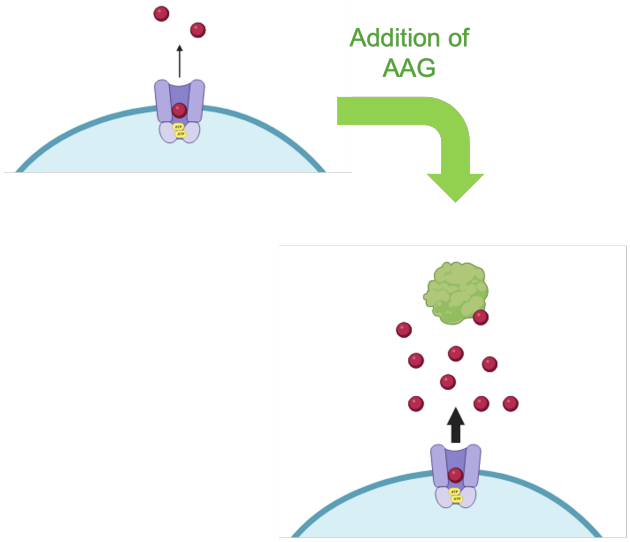

Figure 1.7 – Schematic representation of AAG enhancing transport of substrates by ABCG2. ABCG2 (purple) efflux of substrates (red) without AAG (green) is represented by the top image. Predicted ABCG2:AAG interactions is depicted in the bottom image, where it is hypothesized that AAG would increase ABCG2 efflux.

1.3.2 EMMPRIN; a Possible ABCG2 Interacting Protein

Since MDR stemming from ABCG2 is often caused by overexpression of the transporter, a protein-protein interaction that influences ABCG2 expression was also decided to be investigated for this project. Extracellular matrix metalloproteinase inducer (EMMPRIN), also known as CD147 or basigin (BSG), is a glycoprotein found on the surface of tumour cells that activates the production of matrix metalloproteinases (MMPs) such as in medulloblastoma (Jackson et al., 2023). MMPs are known to facilitate tumour cell invasion, leading to tumour progression and poor patient outcomes. A study by Zhou et al. (2013) investigated ABCG2:EMMPRIN interactions and observed increased ABCG2 expression in the presence of EMMPRIN. Although the researchers could not determine the exact mechanism of ABCG2:EMMPRIN

interactions, they believed that there was a chaperone effect where EMMPRIN either enhanced ABCG2 protein stability at the cell surface or blocked its degradation. Furthermore, they observed that EMMPRIN could bind to ABCG2 to form a complex though its functionality remained unknown. If EMMPRIN does interact with ABCG2, then it would mean that not only does it influence cancer invasion but also MDR, causing it to have a significant two-way role in cancer progression. This potential idea lead to the second question of this project: does EMMPRIN interact with ABCG2, and if so, does it lead to increased expression of ABCG2 (Figure 1.8)?

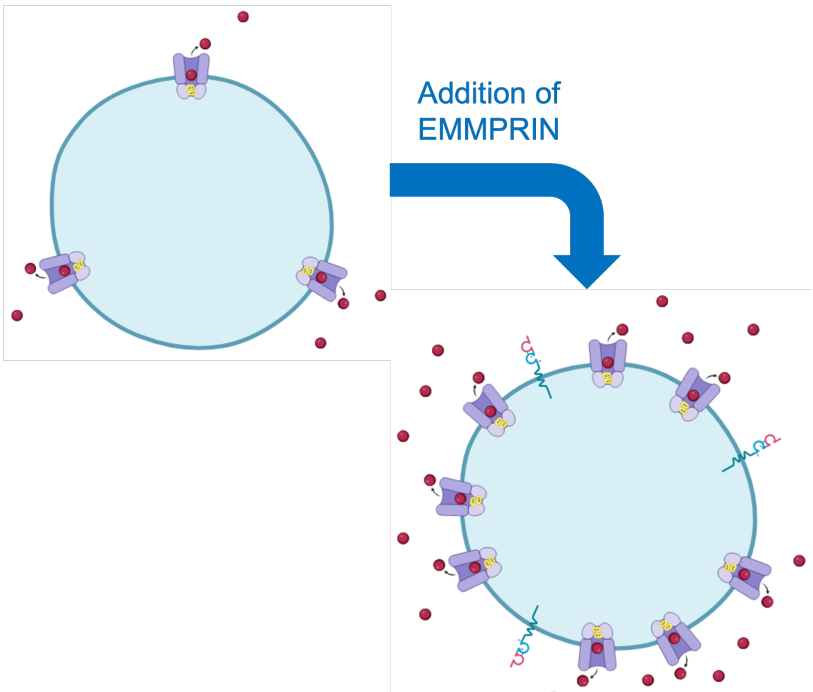

Figure 1.8 – Schematic representation of EMMPRIN enhancing surface cell expression of ABCG2. ABCG2 (purple) is shown effluxing substrates (red) out of the cell without the presence of EMMPRIN in the top image. The bottom image portrays increase ABCG2 expression when EMMPRIN (blue and pink) is co-expressed with it.

1.4 Aims of the Study

As discussed in Section 1.3.1 and Section 1.3.2, two different ABCG2 protein-protein interactions were identified to study for this project to aid in the better understanding of ABCG2-mediated MDR. Studying functional ABCG2:AAG interactions will be performed through transport assays using a cell line stably transfected with ABCG2 to determine any changes in ABCG2 efflux rates. For ABCG2:EMMPRIN functional interactions, cells stably transfected with ABCG2 will be transfected with EMMPRIN for co-expression to determine any increases in ABCG2 expression. In both cases, it would be desirable to be able to directly detect protein-protein interactions, which would require a purification protocol for ABCG2 constructs before any biophysical experiments could be performed.

Chapter 2 Materials and Methods

2.1 Materials and Reagents

Plasmids were received from Sino Biological. All other materials and reagents were obtained from Sigma-Aldrich (Gillingham, UK) or Thermo Fisher Scientific unless stated otherwise.

2.2 Cell Culture and Handling

2.2.1 Maintenance of Adherent Cell Cultures

Cells were grown in either T25 (25 cm^2) or T75 (75 cm^2) flasks at 37°C, 5% CO_2 in Dulbecco's Modified Eagle's Medium (DMEM, 4.5 g/L glucose, 0.58 g/L L-glutamine, 0.11 g/L sodium pyruvate, 3.7 g/L sodium bicarbonate) supplemented with 10% (v/v) HyClone™ foetal bovine serum (FBS, Cytiva) and 1% (w/v) penicillin-streptomycin (P/S, 100 U/mL penicillin, 100 µg/mL streptomycin). Stably transfected cell lines with the Zeocin™ resistance gene were supplemented with 40 – 50 µg/mL of the antibiotic. Cells were passaged, usually twice weekly, when they reached approximately 80 – 90% confluency based on visual inspection. Media was removed through aspiration before cells were washed once with pre-warmed phosphate buffered saline (PBS, Corning) and then incubated in 0.5 – 1 mL trypsin/EDTA for 5 – 15 minutes at 37°C. Once the cells were detached from the flask surface, the trypsin/EDTA was quenched with 3.5 – 4.5 mL media and the cells were centrifuged at 500 x g for 5 minutes. The cell pellets were then resuspended in fresh media and used to seed new flasks at various

dilutions (anywhere from 1/3 to 1/40) depending on the cell growth speed and requirement of planned experiments at the time.

2.2.2 Large-scale Production of Adherent Cell Cultures and Harvest

For large-scale production of ABCG2 expression for protein purification, previously established HEK293T cells stably transfected with sfGFP-ABCG2 and clonally selected to be high expressing were used (Wong, 2015). Cells were grown in DMEM supplemented with 10% (v/v) FBS, 1% (w/v) P/S, and 40 – 50 ug/mL Zeocin™ at 37°C, 5% CO_2. Either 150 mm dishes (145 cm^2) or 500 cm^2 dishes were seeded from T75 flasks at 1/6 – 1/8 dilutions. Once cells visually reached around 90% confluency, media was removed by aspiration before the cells were then exposed to 10 – 40 mL ice-cold PBS for easier detachment. Cells were removed from the dish surface with a cell scraper into a pre-weighed 50 mL conical tube and centrifuged at 1,000 x g, 4°C for 15 minutes. The supernatant was decanted before the cells were resuspended in 10 mL ice-cold PBS and centrifuged again at 1,000 x g, 4°C for another 15 minutes. The supernatant was poured off and then the cell pellet was weighed before being stored at -80°C.

2.2.3 Maintenance and Harvest of Large-scale Suspension Cultures

For even greater yields of protein expression, HEK293T cells stably transfected with His-sfGFP-ABCG2 (established by Horsey et al. (2020)) were grown. Despite traditionally being adherent cells, this cell

line had been adapted to grow in suspension. Cells were grown in DMEM supplemented with 10% (v/v) FBS, 1% (w/v) P/S, 0.1% (w/v) pluronic f-68, 0.25% (w/v) Peptone Primatone® RL, and 40 – 50 ug/mL Zeocin™ at 37°C, 5% CO_2 as similarly described in Mitchell-White et al. (2024). All suspension cultures were grown in flat-bottomed round borosilicate flasks sealed loosely with a foil cap and shaken on an orbital platform set at 180 RPM. 10 mL cultures in 50 mL flasks were first seeded from T25 flasks at a cell density of 2.5 x 10^5 cells/mL. After 3 – 4 days, these cultures were expanded into 40 mL cultures in 100 mL flasks at 5 x 10^5 cells/mL. Typically, these would then seed 80 mL cultures in 250 mL flasks at 2.5 x 10^5 cells/mL after another 3 – 4 days. Finally, cells were expanded to 300 mL cultures in 1 L flasks at 2.5 x 10^5 cells/mL and at least one 300 mL culture was always maintained for seeding more cultures. Once a 300 mL culture reached the cell density of 3 – 4 x 10^6 cells/mL, 10 mM sodium butyrate was added to increase protein expression (Goehring et al., 2014) and then harvested 24 hours afterwards.

To harvest the 300 mL cultures, they were transferred into 400 mL centrifuge tubes and centrifuged at 1,000 x g, 4°C for 15 minutes. The supernatant was removed, and each cell pellet was moved to a pre-weighed 50 mL conical tube and resuspended in 50 mL ice-cold PBS. Cells were then centrifuged in a tabletop centrifuge at 1,000 x g, 4°C for 15 minutes and the supernatant was poured off before the cell pellets were weighed and stored at -80°C.

2.2.4.1 Small-scale Transfections

To determine the effect that EMMPRIN had on ABCG2 expression, a time-course transfection experiment was conducted using an established low expressing HEK293T cell line stably transfected with sfGFP-ABCG2 (Wong et al., 2016). 6-well plates were first seeded at 1.5 x 10^5 cells/mL. After 24 hours, the media was replaced with low serum media (DMEM, 2.5% (v/v) FBS, 1% (w/v) P/S) about 3 hours before transfection. Linear polyethyleneimine (PEI) was used to transfect cells at an approximate PEI nitrogen:DNA phosphorus ratio of 15:1 to introduce cells to DNA (Boussif et al., 1995). Cells were transfected with 2 or 4 µg of pCMV3-Flag-BSG (EMMPRIN) for between 24 and 72 hours. Control cells either remained untransfected or transfected with a membrane protein encoded by a similar size cDNA (CD86) that was not thought to interact with ABCG2. Transfections were carried out in collaboration with Dilraj Dhamrait (School of Life Sciences, University of Nottingham).

2.2.4.2 Large-scale Transfections

In order to obtain enough membranes for direct observation of EMMPRIN:ABCG2 interaction, high expressing HEK293T-sfGFP-ABCG2 cells were seeded in either 150 mm dishes or 500 cm^2 dishes at 3 x 10^5 cells/mL. Approximately 24 hours after seeding, media was changed to DMEM supplemented with 2.5% (v/v) FBS and 1% (w/v) P/S. 3 hours later, cells were transfected using PEI at a nitrogen:phosphate ratio of 15:1 with either EMMPRIN or CD86. 30 µg (for 150 mm dishes) or 104 µg (for 500 cm^2) of DNA was first diluted

with 200 µL distilled water before PEI was added, and the transfection mixtures were added to cells in a dropwise fashion. After 24 hours, the media was replaced with higher serum media (10% (v/v) FBS) and cells were harvested at 48 hours after transfection. See Section 2.2.2 for how cells were harvested.

2.2.5 Poly-L-lysine Treatment

To ensure cell attachment to plate surfaces for transport assays and cloning by limiting dilution, poly-L-lysine was used. The adsorbed poly-L-lysine layers on the treated surfaces are cationic and form ionic interactions with the negatively charged cell membrane (Mazia et al., 1975). 10 µg/mL poly-L-lysine solutions were made from 5 mg/mL stock solutions diluted with distilled water and used to coat the surface of various plate sizes. Treated plates were incubated at 37°C for 1 hour before the poly-L-lysine was aspirated. Plate surfaces were then washed once with PBS and left in fresh PBS until cells were ready for seeding.

2.2.6 Flow Cytometric Cell Sorting

For downstream experiments it was believed that it would be beneficial to derive low-expressing and high-expressing cells from a heterogeneous stable cell line previously established (HEK293S cell line stably transfected with TwinStrep-SNAP-ABCG2 (Mitchell-White et al., 2024)). To do this in a fast and efficient manner, flow cytometry was performed. Resuspended cells were labelled in media (DMEM, 10% (v/v) FBS, 1% (w/v) P/S) supplemented with 2 µM SNAP-Cell® Oregon

Green® (New England Biolabs) for 30 minutes at 37°C, 5% CO_2. Next, they were centrifuged at 300 x g for 5 minutes and then washed once with media absent of the labelling substrate before being pelleted at 300 x g for an additional 5 minutes. Cells were resuspended in fluorescence-activated cell sorting (FACS) buffer (phenol-red free DMEM, 1% (w/v) filter sterilized bovine serum albumin (BSA)) at approximately 1 x 10^7 cells/mL. The cells were then sorted by fluorescence using the Beckman Coulter Astrios EQ Cell Sorter (channel 488).

To collect the desired cell populations from the cell sorter, side scatter area (channel 488-SSC-Area) was plotted against forward scatter area (channel 488-FSC1-Area) and was gated to separate live cells from any debris in the suspension. Side scatter height (channel 488-SSC-Height) of the live cells was then plotted against side scatter width (channel 488-SSC-Width) and gated to divide the single cells from the doublets. Finally, the side scatter area of the monodispersed cells was plotted against fluorescence intensity at 488 nm and gated to separate the 20% lowest and highest fluorescent cells from the remaining cell population. These two populations were independently collected in containers with FACS buffer. Cells were then seeded into a 96-well plate and left to recover at 37°C, 5% CO_2.

2.2.7 Cloning by Limiting Dilution

An alternative to flow cytometric cell sorting to separate cells based on expression levels of ABCG2 for the HEK293S-TwinStrep-SNAP-ABCG2 cell line was limited dilution. A 96-well plate was pre-treated

with poly-L-lysine (see Section 2.2.5) before being seeded up to a theoretical maximum of 2 cells/well in media (DMEM, 10% (v/v) FBS, 1% P/S). Wells were observed by microscopy every other day until there were clear colonies established from a single cell in twelve individual wells. Once these twelve colonies reached around 80 – 90% confluency, they were moved to a 12-well plate pre-treated with poly-L-lysine and introduced to media supplemented with 40 – 50 µg/mg Zeocin™. After about a week, the same colonies were then moved into 6-well plates. Once the colonies reached 80 – 90% confluency in the 6-well plates, media was aspirated from wells and cells were suspended in 1 mL freezing media (90% (v/v) FBS, 10% (v/v) DMSO). Each colony was frozen slowly in their own respective cryotube at -80°C in a pre-cooled Mr. Frosty™ for temporary storage to be taken out later and labelled with a SNAP-tag substrate to determine expression levels.

2.3 Plasmid Preparation

To ensure that the correct plasmids were received for transfections (Section 2.2.4.1 and Section 2.2.4.2), DNA inserts were validated by Sanger sequencing using universal forward and reverse primers (Table 2.1). Sequencing samples were sent to the DNA Sequencing Facility (School of Life Sciences, University of Nottingham, Nottingham, UK). Once sequencing was confirmed, the QIAGEN Plasmid Maxi Kit and its protocol was used to generate the required amount of DNA needed for transfections. Concentration and purity of plasmids were determined using the Nanodrop™ 2000 (Thermo Scientific). DNA purity was evaluated through the A_{260}/A_{280} ratio and only plasmids with an

A_{260}/A_{280} ratio greater than 1.7 was used. Plasmid preparation was done in collaboration with Deborah Briggs (School of Life Sciences, University of Nottingham).

Table 2.1 – Universal primers used to confirm sequencing of plasmids.

Primer Name	Length (bp)	Sequence
T7	20	TAATACGACTCACTATAGGG
BGH reverse	18	TAGAAGGCACAGTCGAGG

2.4 Monolayer Transport Assays

2.4.1 Transport Assay with Mitoxantrone and Ko143

A 96-well black, clear bottom plate (Greiner) was pre-treated with poly-L-lysine (see Section 2.2.5). Three columns of the plate were seeded with 200 µL of untransfected HEK293T cells at 4 – 5 x 10^5 cells/mL. Similarly, three additional columns were seeded with high expressing HEK293T-sfGFP-ABCG2 cells at the same density. Once cells reached 100% confluency confirmed through microscopy, media was removed by aspiration and replaced with 200 µL transport assay reagents, and cells were incubated for 1 hour at 37°C, 5% CO_2. For both cell lines, a column of cells received either 0.04% (v/v) DMSO (solvent control column), 8 µM mitoxantrone (MX, substrate only column), or 8 µM mitoxantrone with 0.5 µM Ko143 (substrate with inhibitor column). All solutions were prepared in phenol-red free, serum-free Hank's balanced salt solution (HBSS) supplemented with 25 mM glucose. After the 1-hour incubation period, the solutions were aspirated out and cells

were washed carefully twice with ice-cold PBS supplemented with 1 mM $MgCl_2$ and 0.1 mM $CaCl_2$ (PBS/Mg^{2+}/Ca^{2+}). Cells were then fixed with 4% (w/v) paraformaldehyde (PFA) for 5 minutes. Fixed cells were washed once with PBS/Mg^{2+}/Ca^{2+} before being left in 200 µL fresh PBS/Mg^{2+}/Ca^{2+}. Using the SpectraMax iD3 microplate reader, an endpoint mitoxantrone fluorescence reading (excitation 607 nm, emission 684 nm) was taken. Background fluorescence was accounted for by subtracting the average DMSO fluorescence from each datapoint of the same cell line. Datapoints with the same conditions were then averaged and compared with averages from other conditions as described in figure legends (Section 3.1.1).

2.4.2 Time-course Transport Assay with AAG

96-well black, clear bottom plates were pre-treated with poly-L-lysine (see Section 2.2.5). The top three rows of each plate were seeded with 200 µL of untransfected HEK293T cells at 4 – 5 x 10^5 cells/mL while the bottom three rows were seeded with high expressing HEK293T-sfGFP-ABCG2 in a similar manner. When cells reached 100% confluency through visual inspection, media was aspirated from wells and cells were washed once with PBS/Mg^{2+}/Ca^{2+}. Cells were deenergized by incubation in 200 µL of 5 mM 2-deoxy-D-glucose (2DG) in PBS/Mg^{2+}/Ca^{2+} for 10 minutes at 37°C. A column of cells not de-energized was used as the solvent control column where cells were exposed to 200 µL 0.04% (v/v) DMSO instead. After 10 minutes, 50 µL of 40 µM mitoxantrone in PBS/Mg^{2+}/Ca^{2+} was added dropwise to the de-energized cells in the same medium (final concentration of

mitoxantrone = 8 μM) and cells were incubated at 37°C, 5% CO_2 for 50 minutes to enable baseline maximal MX accumulation to be determined. All cells were then washed once with PBS/Mg^{2+}/Ca^{2+} before kept moist in 200 μL PBS/Mg^{2+}/Ca^{2+} while a mitoxantrone fluorescence reading (excitation 607 nm, emission 684 nm, referred to as F_{max}) was taken using the SpectraMax iD3 microplate reader.

To initiate efflux, PBS/Mg^{2+}/Ca^{2+} was quickly aspirated from wells and replaced by 200 μL of either HBSS (supplemented with 25 mM glucose), HBSS + 0.5 μM Ko143, HBSS + 5 μM AAG, or HBSS + 5 μM AAG + 0.5 μM Ko143. All transport assay reagents were prepared in phenol-red free, serum-free HBSS supplemented with 25 mM glucose. The solvent control column was reintroduced to 200 μL 0.04% (v/v) DMSO. Cells were then incubated at 37°C, 5% CO_2 for either 30, 45, 60, 90, 120, or 180 minutes. Once cells had finished incubating, they were washed once with ice-cold PBS/Mg^{2+}/Ca^{2+} before being fixed with 4% (w/v) PFA for 5 minutes. Fixed cells were then washed once with PBS/Mg^{2+}/Ca^{2+}. Cells were left in fresh 200 μL PBS/Mg^{2+}/Ca^{2+} and an endpoint mitoxantrone fluorescence reading was taken as the fluorescence after efflux was initiated at a specific timepoint, F_t.

Background fluorescence was accounted for by subtracting the average DMSO fluorescence from each datapoint of the same cell line. The difference in fluorescence between maximum and efflux fluorescence from the same well was compared by dividing the efflux over maximum fluorescence (F_t/F_{max}). Ratios from the same timepoints were then compared together and all ratios were plotted over time after

efflux initiation. A nonlinear regression one-phase decay curve fit was calculated to determine rate constants, and these were compared through a comparison of fits.

2.5 SDS-PAGE and Western Blotting

Cell pellets were harvested and lysed in collaboration with Dilraj Dhamrait while protein assays, SDS-PAGE, and western blots were done in collaboration with Deborah Briggs.

2.5.1 Cell Harvest and Lysis

Cells were washed once with PBS and then harvested in ice-cold PBS. They were centrifuged at 500 x g for 5 minutes and the supernatant was discarded before the cell pellets were stored at -20°C for short-term storage. When ready for use, pellets were resuspended in 250 µL PBS supplemented with 10% (v/v) glycerol and EDTA-free protease inhibitor cocktail set III (Merck) diluted 1:100. Cells were lysed by probe sonication by three pulses of 10 interrupted by 30 second pauses on ice.

2.5.2 Protein Assay

A modified Lowry assay (Bio-Rad) was performed whenever necessary to determine protein concentrations for equal protein loading in sodium dodecyl sulphate-polyacrylamide gel electrophoresis (SDS-PAGE) and western blot analysis. The Bio-Rad DC protein assay kit was used along with a standard curve of 5 – 10 µg BSA. Protein concentrations from cell lysates were calculated by comparing against this standard curve.

2.5.3 Sample Preparation and SDS-PAGE

SDS-PAGE was conducted through modifications of the Laemmli method (Laemmli, 1970). 25 µg of cell lysates were prepared in protein loading buffer (50 mM Tris base pH 6.8, 10% (v/v) glycerol, 2% (w/v) SDS, 0.1% (w/v) bromophenol blue, 5% (v/v) 2-mercaptoethanol) and heated at 37°C for 30 minutes. 10% (w/v) acrylamide resolving gels (375 mM Tris base pH 8.8, 0.1% (w/v) SDS, 0.15% (w/v) ammonium persulfate (APS), 0.06% (v/v) tetramethylethylenediamine (TEMED)) and 4% (w/v) acrylamide stacking gels (125 mM Tris base pH 6.8, 0.1% (w/v) SDS, 0.15% (w/v) APS, 0.06% (v/v) TEMED) were made and placed in gel electrophoresis tanks filled with protein running buffer (25 mM Tris base, 192 mM glycine, 3.5 mM SDS). Prepared samples were loaded into the gels along with a molecular weight marker (SeeBlue™ Plus2 Pre-stained Standard) and electrophoresed at a constant current of 30 mA until the loading buffer had eluted into the tank. Gels were then removed from tanks and used in western blotting (Section 2.5.4) for protein analysis.

2.5.4 Western Blot Analysis

Protein samples that were run on polyacrylamide gels through SDS-PAGE (Section 2.5.3) were transferred onto nitrocellulose membranes. The transfer was completed in a transfer tank filled with western transfer buffer (25 mM Tris base, 192 mM glycine, 20% (v/v) methanol) through electrophoresis at a constant current of 200 mA for 2 hours or 30 mA overnight at 4°C as first introduced by Towbin et al. (1979). Once successful transfer was achieved, the blots were briefly washed

in PBS supplemented with 0.1% (v/v) Tween-20 (PBS/T) before incubating in 5% (w/v) non-fat milk (Marvel) dissolved in PBS/T for 1 hour at room temperature on rotator. This was to prevent non-specific binding of the primary antibodies. The membranes were then cut horizontally at around the 64 kDa molecular weight marker to separate the blots of the protein of interest from the loading control protein. All blots were incubated with their respective primary antibody (see Table 2.2) for either 2 hours at room temperature or overnight at 4°C, rotating. Blots were then washed three times with PBS/T (5 minutes per each wash) for the removal of any unbound primary antibody before incubating in their respective secondary antibody (see Table 2.2) for 1 hour rotating at room temperature. A further three, 5-minute washes in PBS/T were performed on the blots. For blots that were incubated with a horseradish peroxidase (HRP) conjugated secondary antibody, they were additionally incubated with the enhanced chemiluminescence reagent (ECL, SuperSignal™ West Pico PLUS Chemiluminescent Substrate) for 1 minute. All blots were imaged using the Bio-Rad ChemiDoc MP Imaging System.

Table 2.2 – Antibodies used in western blots.

Antibody	Primary/ Secondary	Host Species	Dilution	Source
BXP-21	Primary	Mouse, monoclonal	1:500	Sigma-Aldrich
Anti-FLAG	Primary	Rat, monoclonal	1:2,000	Invitrogen
Anti-β-actin (loading control)	Primary	Mouse, monoclonal	1:2,000/ 1:5,000	Sigma-Aldrich
IRDye® 800CW anti-mouse IgG	Secondary	Donkey, polyclonal	1:10,000	Li-Cor
Peroxidase HRP-conjugated anti-rat	Secondary	Rabbit, polyclonal	1:2,000	Dako

2.5.5 Densitometric Analysis of Band Intensity

To analyse band intensities from western blots, the Fiji (ImageJ) software was used. Bands were identified using the rectangle tool and their intensities were plotted (Analyse>Gels>Plot Lanes). With the wand (tracing) tool, the area from each peak was obtained. To compare protein densities from different lanes and blots, the relative density was calculated by dividing the area of the sample peak with the area of the respective loading control peak. Relative densities were plotted with bar graphs and significance was calculated using two-way ANOVA analyses.

2.6 Preparation of Membranes and Protein Purification

All protein purification and size-exclusion chromatography (SEC) was conducted at the Membrane Protein Lab (MPL, Diamond Light Source Ltd, Didcot, UK) in collaboration with Dr. Andrew Quigley and Dr. Harish Cheruvara.

2.6.1 Preparation of Membranes

Thawed cell pellets harvested from large-scale production of adherent cell cultures (Section 2.2.2) and transfections (Section 2.2.4.2) were resuspended in 10 mL of ice-cold membrane isolation buffer (MIB1, 50 mM Tris pH 7.4, 250 mM sucrose, 0.2 mM $CaCl_2$) per 1 g of cells supplemented with EDTA-free protease inhibitor cocktail set III diluted to 1:50. Cell pellets from large-scale suspension cultures (Section 2.2.3) were resuspended in 5 mL of ice-cold MIB1 per 1 g of cell that was supplemented with EDTA-free protease inhibitor cocktail set III diluted to 1:100.

Adherent cells were lysed using a nitrogen cavitation vessel (Parr Instrument Company) that was pre-cooled on ice. Once the resuspended cells were poured into the cavitation vessel and sealed, it was attached to a nitrogen gas cylinder. Cells were pressurized at 1,000 psi within the vessel for 15 minutes while on ice. Pressure was then released slowly while the lysed cells were collected from the vessel. Samples were re-added to the vessel and the process was repeated.

Resuspended suspension cells were lysed using a continuous flow cell disruptor (Constant Systems) due to the larger volume of resuspensions (175 – 200 mL). The disruptor was pre-cooled with tap water through its cooling jacket before resuspended cells were added through the inlet reservoir and lysed at a pressure of 10 – 30 kpsi. Samples were collected from the output tubing and reapplied to the disruptor for a second passage.

Once cells were lysed, they were centrifuged at 2,500 – 3,000 x g for 15 – 30 minutes at 4°C to remove debris, nuclear material and any unbroken cells. The supernatant was then transferred into pre-weighed ultracentrifuge tubes and centrifuged at 100,000 x g for 1 hour at 4°C. The supernatant was carefully removed, and the cell membrane pellets were weighed. They were subsequently resuspended at 100 – 200 mg of wet membrane per mL in membrane isolation buffer 4 (MIB4, 50 mM 4-(2-hydroxyethyl)-1-piperazineethanesulfonic acid (HEPES), 5% (v/v) glycerol) supplemented with EDTA-free protease inhibitor cocktail set III diluted to 1:100. To ensure that membrane pellets were resuspended thoroughly, they were first sheared through a broad-gauge needle (20G) five times, then through a narrow-gauge needle (25G) twenty times. Cell membranes were flash frozen on dry ice and stored at -80°C.

2.6.2 Protein Purification with Detergent Screen Detergents

Before large-scale purifications of sfGFP-ABCG2 constructs could be performed, the detergent that would best solubilize and purify ABCG2

needed to be determined for large-scale purification. To do this, membrane preparations (sfGFP-ABCG2, sfGFP-ABCG2 co-transfected with EMMPRIN, and sfGFP-ABCG2 co-transfected with CD86) were solubilized and purified in 12 different detergents and screened through SDS-PAGE (Section 2.6.3) and fluorescence-detection size-exclusion chromatography (FSEC) (Section 2.6.4).

Table 2.3 – Detergent concentrations used for membrane protein solubilization and purification screening.

Detergent/Additive	Extraction Concentration (w/v)	CMC (w/v)
DDM	1%	0.0087%
DDM + CHS	1% + 0.2%	0.0087% + 0.0033%
DM	1%	0.087%
DM + CHS	1% + 0.2%	0.087% + 0.0033%
OG + CHS	1.5% + 0.2%	0.53% + 0.0033%
LMNG	1%	0.001%
OGNG + CHS	1% + 0.2%	0.058% + 0.013%
LDAO	1%	0.023%
C12E8	1%	0.0048%
C12E9	1%	0.003%
Cymal-5	1%	0.12%
Fos-choline-12	1%	0.047%

Membranes were first resuspended in 12 mL lysis buffer (50 mM HEPES pH 7.5, 500 mM NaCl, 5% (v/v) glycerol, 10 mM imidazole pH 7.5, cOmplete™, EDTA-free protease inhibitor cocktail (Roche)). Resuspended membranes were then added into a 96-well deep well block with the screening detergents at final concentrations indicated in

Table 2.3. The deep well block was sealed with foil to prevent spillage and shaken at 450 RPM, 4°C for 1 hour. The block was then centrifuged at 3,500 x g for 30 minutes at 4°C. The supernatant was transferred into a new 96-well deep well block and 50 µL of equilibrated resin (Strep-Tactin®XT 4Flow® (iba)) supplemented with 100 µg biotinylated anti-GFP nanobody (made at Diamond Light Source Ltd) was added to every well. The block was foil-sealed and shaken at 1,000 RPM, 4°C for 1 hour to allow for the solubilized sfGFP-ABCG2 to bind to the resin. The solubilized sfGFP-ABCG2 and resin mixtures were then transferred to a 96-well polypropylene filter plate (Crawford Scientific) and flow through was collected. Wells were washed with wash buffer (50 mM HEPES pH 7.5, 500 mM NaCl, 5% (v/v) glycerol) supplemented with 3 x critical micelle concentration (CMC) of their respective detergent (Table 2.3) and centrifuged at 300 x g, 4°C for 1 minute. The wash step was repeated twice more. A final centrifugation of the plate was performed at 500 x g, 4°C for 3 minutes to remove any excess wash buffer. Proteins specifically bound to the GFP-nanobody were eluted by addition of 50 µL of elution buffer (50 mM HEPES pH 7.5, 500 mM NaCl, 5% (v/v) glycerol, 50 mM biotin, 3 x CMC of detergent) to the resin. After incubating for 20 minutes at 4°C, the filter plate was then centrifuged at 500 x g, 4°C for 3 minutes with eluted proteins collected into a new 96-well plate.

2.6.3 SDS-PAGE for Protein Purification

10 µL of purified proteins from Section 2.6.2 were loaded onto pre-cast NuPAGE™ 4 – 12% Bis-Tris midi protein gels and electrophoresed in

NuPAGE™ MES (2-(N-Morpholino)ethanesulfonic acid) SDS running buffer at a constant current of 30 mA for 70 minutes. Samples were loaded alongside Benchmark™ Fluorescent Protein Standard and SeeBlue™ Pre-stained Protein Standard as molecular weight markers. Gels were then briefly washed with distilled water once and images were taken for fluorescence with a ChemiDoc MP Imaging System before stained with InstantBlue™ (Expedeon) for 1 hour at room temperature, rocking. Stained gels were rinsed with distilled water and imaged once more.

2.6.4 FSEC for Detergent Screen

Purified proteins eluted for the detergent screen (Section 2.6.2) were injected onto an SRT-C-300 HPLC (high-performance liquid chromatography) column (Sepax) connected to a 3 mL SRT-C 300 guard column (Sepax). Samples were run overnight with filtered and degassed SEC buffers (50 mM HEPES pH 7.5, 500 mM NaCl) supplemented with 2 x CMC of detergents (Table 2.3) at a flow rate of 1.0 mL/min at 4°C. UV absorbance and GFP fluorescence (excitation 488 nm, emission 507) were measured as protein fractions eluted over time, and fluorescence measurements were exported to GraphPad Prism to plot spectra. The FSEC spectrum for each construct was then used to determine the best detergent to use for large-scale protein purification (Section 2.6.5).

2.6.5 Large-scale Purification of ABCG2 Constructs

Membranes of the same constructs were pooled together and resuspended in lysis buffer (50 mM HEPES pH 7.5, 500 mM NaCl, 2.5% glycerol, cOmplete™, EDTA-free protease inhibitor cocktail, 1% (w/v) DDM) for a total volume of 50 mL and rotated for 1 hour at 4°C. Soluble and insoluble proteins were separated through ultracentrifugation at around 200,000 x g, 4°C for 45 minutes. The supernatant containing the soluble proteins was then transferred to a new 50 mL conical tube and incubated with 2 mL of equilibrated resin (Strep-Tactin®XT 4Flow®) supplemented with 4 mg of biotinylated anti-GFP nanobody for either 1 hour or overnight at 4°C, rotating. The membrane and resin mixture was added to a gravity column and washed with 10 times the column volume with wash buffer (50 mM HEPES pH 7.5, 500 mM NaCl, 2.5% (v/v) glycerol, 0.03% (w/v) DDM) at 4°C. Membrane proteins were subsequently eluted from the column with elution buffer (50 mM HEPES pH 7.5, 500 mM NaCl, 2.5% glycerol, 0.03% (w/v) DDM, 50 mM biotin) and collected as 1 mL fractions at 4°C.

The A_{280} UV-absorbance of protein elution fractions were measured on a Nanodrop™ 2000 to determine which fractions had the highest concentration of protein. The most concentrated fractions were pooled together and transferred to a concentrator with a 100 kDa molecular weight cut off (MWCO) and centrifuged at 3,000 x g, 4°C until the protein volumes were reduced to 500 µL. SEC was then performed by injecting the concentrated protein onto a Superdex™ 200 Increase

10/300 GL column (Cytiva) using an ÄKTApurifier (Cytiva). Samples were run overnight with SEC buffer (50 mM HEPES pH 7.5, 500 mM NaCl, 2.5% (v/v) glycerol, 0.02% (w/v) DDM) at a flow rate of 0.4 mL/min at 4°C and 200 µL fractions were collected in a 96-well deep well block. UV absorbance of the elution fractions was measured throughout a run.

To determine which SEC fractions had purified sfGFP-ABCG2 constructs, samples from fractions correlated with absorbance values above the baseline were electrophoresed through SDS-PAGE as described in Section 2.6.3. Samples from the insoluble and soluble protein before purification, the flow through, wash, and elution fractions from purification, the flow through from protein concentration, and the concentrated protein before SEC were run alongside SEC fractions to appraise how much protein was collected or lost during each step. SEC fractions that appeared have sfGFP-ABCG2 constructs present based on gel results were concentrated to 20 µL with a 100 kDa MWCO Vivaspin® 500 concentrator (Sartorius) at 10,000 x g, 4°C. The concentrated protein was then transferred to a new microcentrifuge tube and centrifuged at 17,000 x g for 10 minutes at 4°C. The UV-absorbance of the supernatant was taken at A_{280} with a Nanodrop™ 2000 to determine protein concentration.

2.7 Data Analysis

Unless other indicated, all experiments were carried out independently at least three times. Numbers of technical and biological repeats are

stated in relevant figure captions. Data analysis was performed using GraphPad Prism and Excel. Where shown, statistical significance was calculated by Student's t-test, by comparison of fits using rate constants calculated by nonlinear regression one-phase decay curve fits, and by two-way ANOVA where multiple experimental groups were compared.

Chapter 3 Results

3.1 Interaction of ABCG2 with AAG

As discussed in the introduction (see Section 1.3.1), one of the hypotheses was that ABCG2 may directly interact with alpha-1-acid glycoprotein (AAG), which would increase the efflux rate of ABCG2. To determine the functional impact of this potential interaction, it was determined that monolayer transport assays would be the best way to investigate. Monolayer assays are readily adaptable to 96-well plates and enable multiple timepoints with replicates within an experiment. Other methods such as flow cytometry would be difficult to perform with the complexity the timepoints bring to the assay. Monolayer assays were developed based on ABCG2 efflux assays described in Mitchell-White et al. (2024) and Horsey et al. (2020).

3.1.1 Transport Assay with Mitoxantrone and Ko143

Before AAG was introduced to the transport assays, first it was important to establish that the cell line stably transfected with ABCG2 was interacting with mitoxantrone (MX) and Ko143 as expected. MX is a fluorescent substrate that ABCG2 is known to efflux out of cells while Ko143 is a non-fluorescent ABCG2 inhibitor. The efflux of MX would be observed with cells expressing functional ABCG2 and in turn intracellular fluorescence would be expected to be low. With Ko143 inhibition, ABCG2 would be unable to transport mitoxantrone out of cells and therefore higher intracellular fluorescence would result. The

HEK293T cells stably transfected with sfGFP-ABCG2 were compared with untransfected HEK293T for this assay.

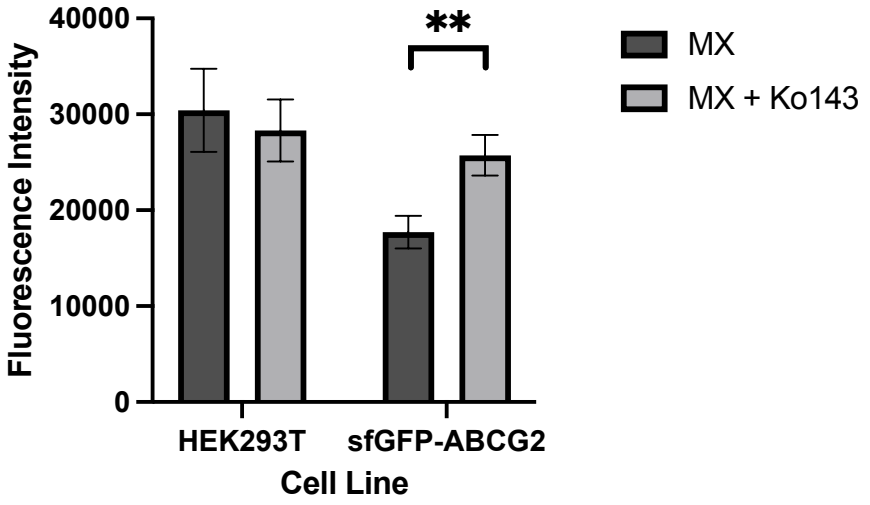

Figure 3.1 – MX transport by ABCG2 in the presence and absence of Ko143. Untransfected HEK293T and stably transfected HEK293T-sfGFP-ABCG2 cells were incubated with MX in the presence or absence of Ko143. Cells were then washed twice before being fixed and MX fluorescence was measured (excitation/emission 607/684 nm). Background fluorescence was removed from each datapoint by subtracting the average DMSO fluorescence before replicate datapoints were averaged. Data was assessed for statistical significance by Student's t-test (** < 0.01) (mean ± SD). Data shown are representative of three separate experiments (n = 3) with 6 replicates for each condition within each experiment.

As expected, the mitoxantrone fluorescence intensity was significantly higher when Ko143 was present in ABCG2 expressing cells (Figure 3.1, $p < 0.01$). In the untransfected cells, the fluorescence intensities were relatively similar whether the inhibitor was present or absent (Figure 3.1). Concluding that the cells were reacting to the assay treatment as theorized, the next step was to design a transport assay that also included the putative activator of ABCG2 transport, AAG.

3.1.2 Time-course Transport Assay with AAG

The goal of the transport assays with AAG was to calculate efflux rates of ABCG2 with and without AAG. Efflux may have a passive component (i.e. diffusion down a concentration gradient) as well as an active component (i.e. ATP hydrolysis mediated). Therefore, to enable comparison between conditions the cells were exposed to, it was important to try to obtain a consistent baseline mitoxantrone fluorescence. To achieve comparable mitoxantrone “loading”, HEK293T and HEK293T-sfGFP-ABCG2 cells were de-energized first through ATP depletion. Since ABCG2 uses ATP hydrolysis to move substrates across the cell membrane, by depleting cells of ATP, ABCG2 pumps are unable to function properly. Using Sajid et al. (2020) for guidance on ATP-depletion, cells were initially incubated in 20 mM 2-deoxy-D-gluose (2DG) and 5 mM sodium azide for the first 10 minutes before the addition of mitoxantrone in the same medium for the next 20 minutes. 2DG is a glucose analogue where the 2-hydroxyl group is substituted with a hydrogen atom, which becomes phosphorylated to 2-deoxy-d-glucose-6-phosphate and is then unable to undergo glycolysis because it cannot isomerize to fructose-6-phosphate (Pajak et al., 2020). Anionic azide inhibits cellular respiration by binding to Fe^{3+} ions in cytochrome oxidase in mitochondria (Ishikawa et al., 2006). Thus, combined 2DG and azide treatment results in inhibition of both glycolysis and oxidative phosphorylation. Initial treatment with both chemicals indicated that the impact was too harsh on the adherent cells; they were washing off the plate surface during the wash steps

before fluorescence readings could be taken. After some optimization, it was determined that incubating the cells solely in 5 mM 2DG for 60 minutes and adding mitoxantrone 10 minutes into that incubation period was best for cellular de-energization and to maximize mitoxantrone exposure, without loss of cell viability (cells remain fully adherent).

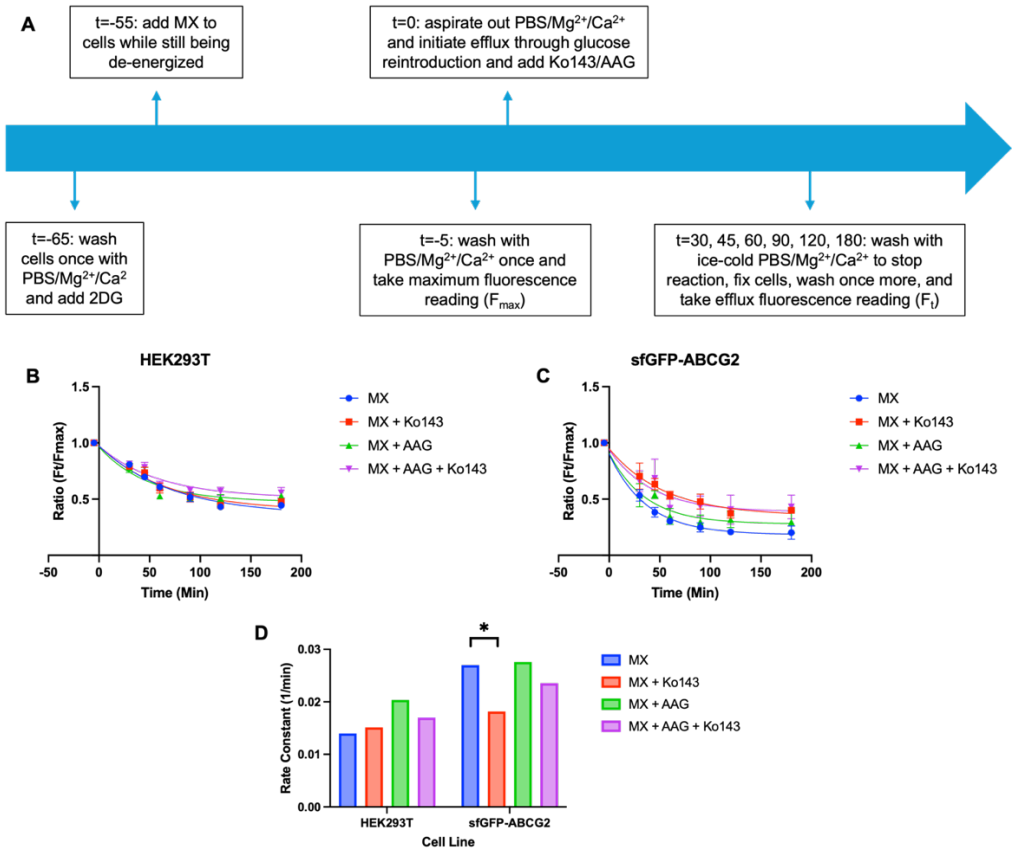

Figure 3.2 – Impact of AAG on efflux of MX by ABCG2. A provides a timeline of the time-course experiments that were performed. Average DMSO fluorescence was subtracted from each datapoint before the fluorescence ratios for both cell lines (**B** and **C)** were calculated at specific efflux timepoints (t) by dividing cellular fluorescence at that time (F_t) by maximum fluorescence (F_{max}) (mean ± SD). These ratios were then plotted over time and a nonlinear regression one-phase decay curve fit was calculated to determine rate constants for each cell line and condition (**D**). A comparison of fits was performed between each condition among the same cell line to determine whether there was any statistical significance (* < 0.05). Data from **B**, **C**, and **D** is from 1 representative experiment (3 replicates for each condition) performed. The experiment was repeated 3 times with similar results.

Initially, a kinetic assay measuring fluorescence in each well at every minute over a 1-hour period was performed to try to measure efflux rates among the different conditions (MX, MX + Ko143, MX + AAG, and MX + AAG + Ko143) introduced to the cells. However, results from the kinetic assay showed very minimal change over the measured time for all conditions (data not shown). Further investigation of this revealed that the plate reader modality was recording both cell-retained MX and effluxed MX (i.e. MX in the well). Therefore, an alternative time-course assay was adopted instead involving a series of wash steps at defined time points (to remove effluxed MX) prior to measuring the remaining intracellular fluorescence (Figure 3.2 A). As expected, there was no difference in efflux rates among the HEK293T cells exposed to different reagents (Figure 3.2 B and D). In other words, AAG did not result in an increase in the rate of efflux of MX from cells that did not express detectable ABCG2. For the cells transfected with sfGFP-ABCG2, those that were only exposed to MX had a significantly faster efflux rate compared to cells exposed to MX + Ko143 (Figure 3.2 C and D, $p < 0.05$), consistent with Ko143 inhibition of MX efflux seen in Figure 3.1. Additionally, this assay showed that there was no increase in ABCG2 efflux when AAG was introduced to sfGFP-ABCG2 cells (Figure 3.2 C and D). Rather, the rate of MX efflux was unaffected with the introduction of AAG and was roughly equal to that of cells that were only exposed to MX. This assay concluded that AAG did not significantly affect the mitoxantrone efflux rate of ABCG2.

3.2 Interaction of ABCG2 with EMMPRIN

With the finding that AAG did not affect MX efflux rate of ABCG2 based on time-course transport assays, the project's focus shifted to the second hypothesis proposed in the introduction: EMMPRIN increases expression levels of ABCG2. Before any experiments could be carried out with EMMPRIN, it was first important to establish cell lines that were either low ABCG2 expressing (for functional experiments) or high ABCG2 expressing (for protein purification for biophysical experiments). A low expressing ABCG2 cell line was required for the functional experiments to easily measure any increases in ABCG2 expression and to have confidence that any observed ABCG2:EMMPRIN interactions were genuine. If ABCG2 expression levels were excessively high during the functional experiments, it would significantly increase the likelihood that any observed ABCG2:EMMPRIN interactions were the result of collisional effect.

A HEK293S-TwinStrep-SNAP-ABCG2 cell line with heterogeneous ABCG2 expression was initially sorted through flow cytometric cell sorting. This cell line was used because the Kerr Lab had an already established purification protocol based upon the TwinStrep tag (Mitchell-White et al., 2024) that could be used for the experiments looking at biophysical interactions between either ABCG2:AAG or ABCG2:EMMPRIN (see Section 3.3). Cells with either 20% of the lowest or highest ABCG2 expression levels in the population (determined through SNAP-Cell® Oregon Green® fluorescence) were sorted and subsequently seeded into a 96-well plate. However, in the

days after flow cytometry, cell viability of the sorted cells dramatically decreased for reasons that were unknown. Flow cytometric cell sorting was attempted three times with the same outcome (data not shown). As an alternative, cells were sorted through cloning by limiting dilution instead. Although this method of cell sorting worked, due to the time constraints of the project, previously established low and high expressing ABCG2 cell lines were eventually used instead. At this point, contact with the Membrane Protein Lab (MPL, Diamond Light Source Ltd, Didcot, UK) had been established and collaborators there conformed that sfGFP-ABCG2 cell lines would also be suitable for biophysical experiments since the fluorescent GFP-tag could be used for protein purification. Given that the Kerr Lab already had low and high expressing clonal cell lines of HEK293T-sfGFP-ABCG2 (Wong, 2015) it was decided to proceed with these.

To test whether ABCG2 expression increases in the presence of EMMPRIN/CD147, stably transfected HEK293T-sfGFP-ABCG2 (low expressing) cells were co-transfected with various amounts of plasmid encoding EMMPRIN/CD147 (0, 2, or 4 μg) and were then harvested 24, 48, or 72 hours after transfection. As a control, cells were co-transfected with plasmids encoding CD86 because it is not known to interact with ABCG2 and has a similar molecular weight (and single transmembrane span) to that of EMMPRIN. Harvested cells were lysed and equivalent amounts of protein separated through sodium dodecyl sulphate polyacrylamide gel electrophoresis (SDS-PAGE) and then analyzed through western blots. Transfections were done in

collaboration with Dilraj Dhamrait (School of Life Sciences, University of Nottingham) while SDS-PAGE and western blots were done in collaboration with Deborah Briggs (School of Life Sciences, University of Nottingham).

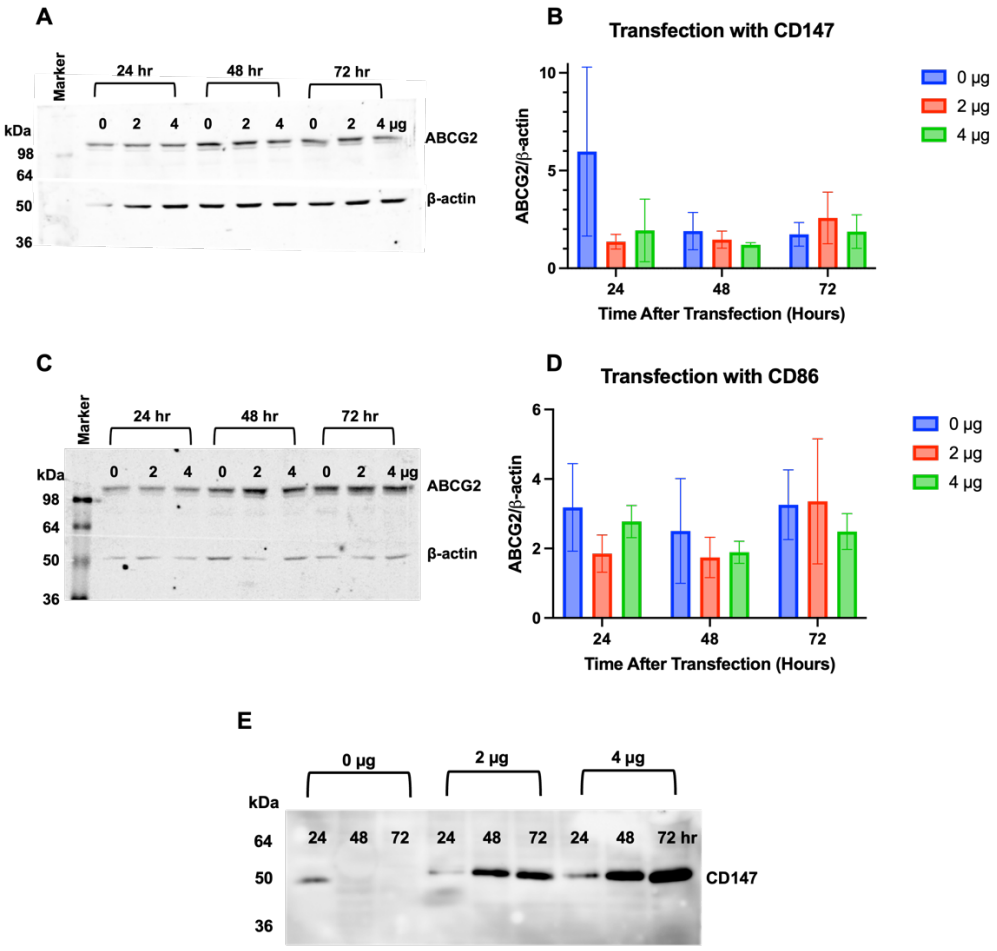

Figure 3.3 – ABCG2 expression outcomes with successful co-transfections of EMMPRIN/CD147 and CD86. Low expressing HEK293T-sfGFP-ABCG2 were co-transfected with either CD147 (EMMPRIN) or CD86 (control) at different DNA quantities (0, 2, or 4 µg). Co-transfected cells were then harvested 24, 48, or 72 hours after transfection. Cells were lysed before loading onto SDS-PAGE gels and run at a constant current of 30 mA before being transferred onto nitrocellulose membranes for western blot analyses. Blots shown in **A** (co-transfected with EMMPRIN/CD147) and **C** (co-transfected with CD86) were incubated with BXP-21 primary antibody (1:500) while blot shown in **E** was incubated with anti-FLAG primary antibody (1:2,000; plasmid encoding EMMPRIN has a N-terminal FLAG tag). Densitometric analysis was performed on blots incubated with BXP-21 primary to quantify ABCG2 expression relative to β-actin (loading control protein) by calculating the ABCG2/β-actin ratios (**B** and **D**, mean ± SD). Two-way ANOVA analyses were carried out to determine any significance from the densitometric data. **A**, **C**, and **E** are representatives of the blots that were run with lysed cells that were transfected with the same conditions. Transfections and western blots were carried out on three separate occasion (n = 3).

Western blots were performed with anti-ABCG2 to monitor ABCG2 protein expression (Figure 3.3A, C) and with anti-actin as a control for protein loading. Parallel blots were also incubated with the primary antibody anti-FLAG to confirm there was protein expression from the co-transfected plasmids to verify the success of the transfections. Based on the bands portrayed in Figure 3.3 E, the co-transfections were successful since both EMMPRIN (CD147) and CD86 (not shown) were expected to have a molecular weight of around 50 kDa.

Blots displayed in Figure 3.3 A and C were used to determine ABCG2 expression levels relative the loading control protein, β-actin, through densitometric analysis (Figure 3.3 B and D). The hypothesis was that since ABCG2 expression is believed to increase in the presence of EMMPRIN, ABCG2 expression relative to β-actin (ABCG2/β-actin) would increase as the amount of EMMPRIN cDNA transfected and harvest time after transfection increased. Furthermore, because CD86 is not known to interact with ABCG2, ABCG2 expression would not increase with exposure to CD86 regardless of time and plasmid quantity. However, ABCG2 expression did not significantly increase with increasing concentrations of EMMPRIN and also did not significantly increase over time post-transfection (Figure 3.3 B). With the CD86 control, there was no significant increase in ABCG2 expression observed which was expected (Figure 3.3 D). Contrary to the hypothesis, these results do not provide evidence that ABCG2 expression is stabilized by interactions with EMMPRIN.

3.3 Protein Purification of ABCG2 Constructs for Biophysical Experiments

Whilst functional experiments were ongoing, biophysical work on ABCG2:AAG and ABCG2:EMMPRIN interactions were running in parallel. This required purified proteins. Due to the hydrophobic character of membrane proteins and their native state of being embedded within the lipid bilayer, they are notoriously difficult to purify. Traditionally, membrane proteins have been solubilized and purified with detergents. These detergents displace the native lipid environment of the membrane proteins (Figure 3.4 A), and the downside is that this leads to loss in any interactions the proteins have with the lipid bilayer that may be essential when studying their structures and functions. Over the past two decades, polymers that form nanodiscs (first described by Bayburt et al., 2002) around membrane proteins to solubilize them have been increasingly used. The advantage that nanodiscs have over traditional detergents is that they provide a more native-like state to the proteins because the proteins are solubilized among small patches of the lipid bilayer (Bayburt and Sligar, 2009) as shown in Figure 3.4 B.

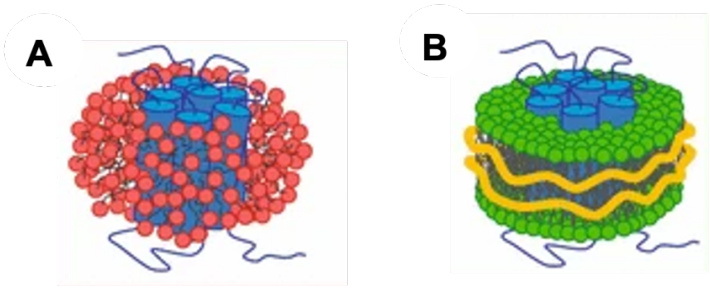

Figure 3.4 – Different methods for how membrane proteins can be solubilized. Protein is indicated in blue, and the lipid bilayer is indicated in green. **A** portrays the protein embedded in a detergent (red) micelle. **B** represents a protein solubilized within a protein nanodisc stabilized by SMA. Figure adapted from Dorr et al. (2016).

Although the Kerr Lab has had past success with purifying ABCG2 using nanodiscs with styrene maleic acid (SMA) and diisobutylene maleic acid (DIBMA), these nanodiscs had eventual undesirable interactions with reagents that disrupted downstream experiments (Horsey, 2018). Thus, more traditional detergents were decided to be used instead for this project. Expertise of ABCG2 solubilization and purification was sought from MPL due to their specialty in high-throughput purification and characterization of membrane proteins. With the MPL's help and use of their facilities and reagents accessible for visiting users, a twelve-detergent screen was first conducted on ABCG2 constructs prepared through membrane preparations. This was to determine which detergent solubilized and stabilized the constructs the best. Membranes from cells expressing either sfGFP-ABCG2 alone, or from cells co-transfected with EMMPRIN or CD86 were employed. Purified wildtype sfGFP-ABCG2 proteins would be used to test biophysical interactions with soluble AAG (procured through Sigma-Aldrich). Meanwhile, EMMPRIN was required to be co-

expressed and then co-purified with sfGFP-ABCG2 through large-scale transfections and purification before any ABCG2:EMMPRIN biophysical interactions could be tested. This was because EMMPRIN is also a membrane protein. CD86 was also co-expressed with sfGFP-ABCG2 as a control to be used for ABCG2:EMMPRIN biophysical interactions since CD86 is a membrane protein with a similar molecular weight to that of EMMPRIN.

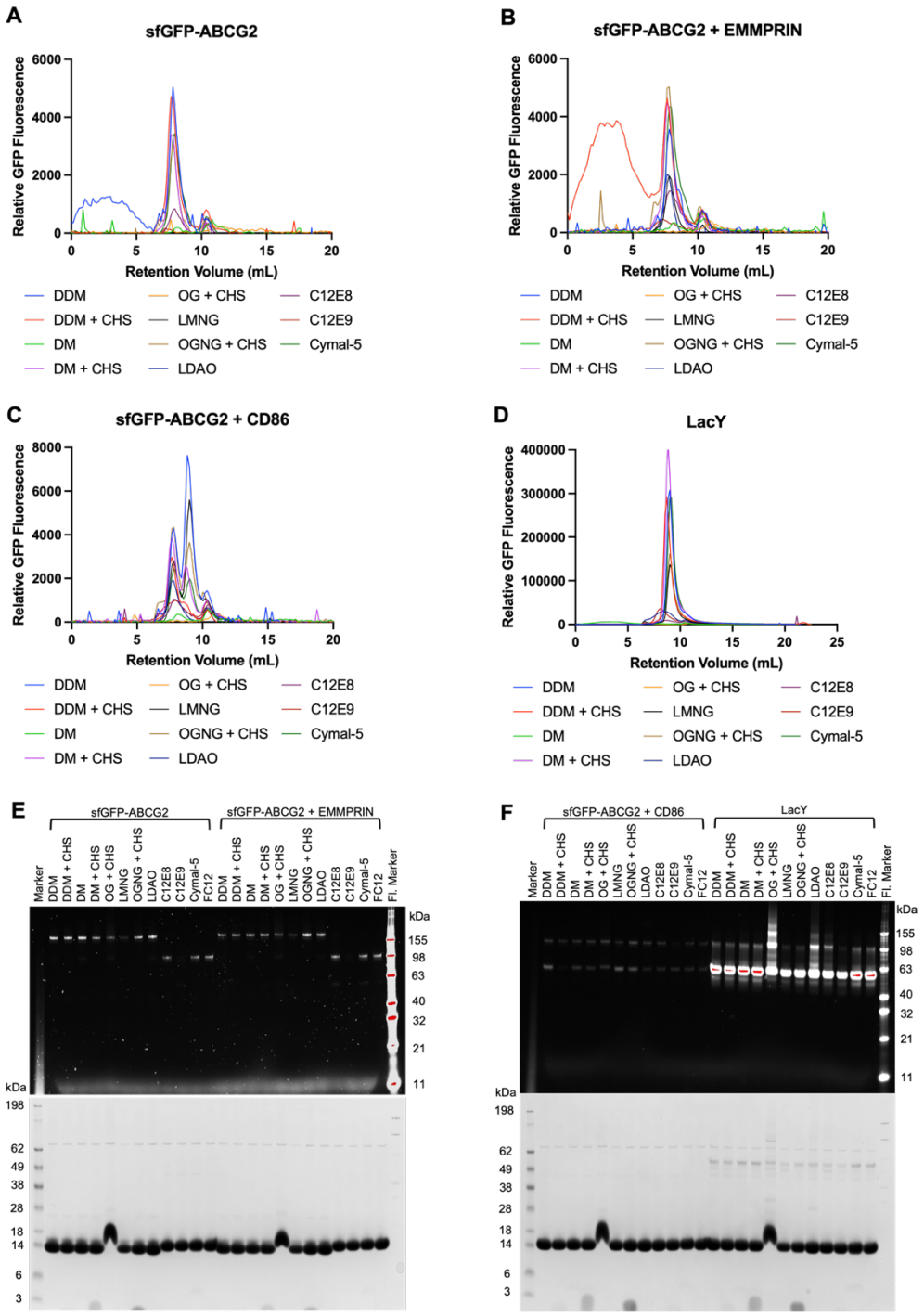

Figure 3.5 – FSEC and SDS-PAGE results from detergent screens. sfGFP-ABCG2 constructs along with a control (GFP-tagged LacY) were solubilized and purified through a twelve-detergent screen and then products were measured through fluorescence-detection size exclusion chromatography (FSEC, **A** – **D**) and SDS-PAGE (**E** and **F**). The gels on the top displayed in **E** and **F** are fluorescent gel images while the bottom gels are images taken after InstantBlue™ staining. Proteins samples purified with fos-choline-12 (FC12) were only run on SDS-PAGE gels to test purify of membrane preparations used for the detergent screens.

Once the sfGFP-ABCG2 constructs were solubilized, they were incubated with biotinylated anti-GFP nanobody that would bind to the sfGFP-tag on the proteins. Solubilized proteins bound with the nanobody were then incubated with a suitable resin before purification was performed. Purified proteins from the detergent screens were analyzed through FSEC and SDS-PAGE (Figure 3.5) to determine which detergents were best for large-scale purifications. Alongside the sfGFP-ABCG2 constructs, a GFP-tagged LacY protein was also subjected to the detergent screen as a control (provided kindly by the MPL). All purified sfGFP-ABCG2 constructs had very low relative GFP fluorescence output from the FSEC (Figure 3.5 A – C) in comparison to the purified LacY proteins (Figure 3.5 D) which had fluorescence signals that were fifty to eighty-folds higher. Furthermore, SDS-PAGE gel results showed low GFP signal from the sfGFP-ABCG2 constructs compared to the LacY proteins (top gels in Figure 3.5 E and F), complimenting the data from the FSEC. Stained gels also portrayed minimal signal from the sfGFP-ABCG2 constructs (bottom gels in Figure 3.5 E and F). The low signals from the constructs of interest signified that ABCG2 protein expression had been low within the HEK293T-sfGFP-ABCG2 cell line used for membrane preparations and would lead to low product yields from large-scale protein purifications.

Despite the low yield outcomes, data from the FSEC was still used to determine which detergent would work best for the large-scale purifications. Relative GFP fluorescence signals from sfGFP-ABCG2 proteins solubilized and purified with DDM were relatively high among

all three constructs (Figure 3.5 A – C). Thus, DDM was the detergent of choice for all large-scale purifications.

Initially, large-scale purification was tested using sfGFP-ABCG2 membranes. However, results from the sfGFP-ABCG2 purification indicated that the incubation time for the solubilized protein with the resin needed to be increase from 1 hour to overnight (data not shown). Because all sfGFP-ABCG2 membrane preparations had been used in the first large-scale purification, sfGFP-ABCG2 co-expressed with EMMPRIN membrane preparations were used for the modified purification. With this method, yield of purified proteins after size-exclusion chromatography (SEC) had increased by six-fold.

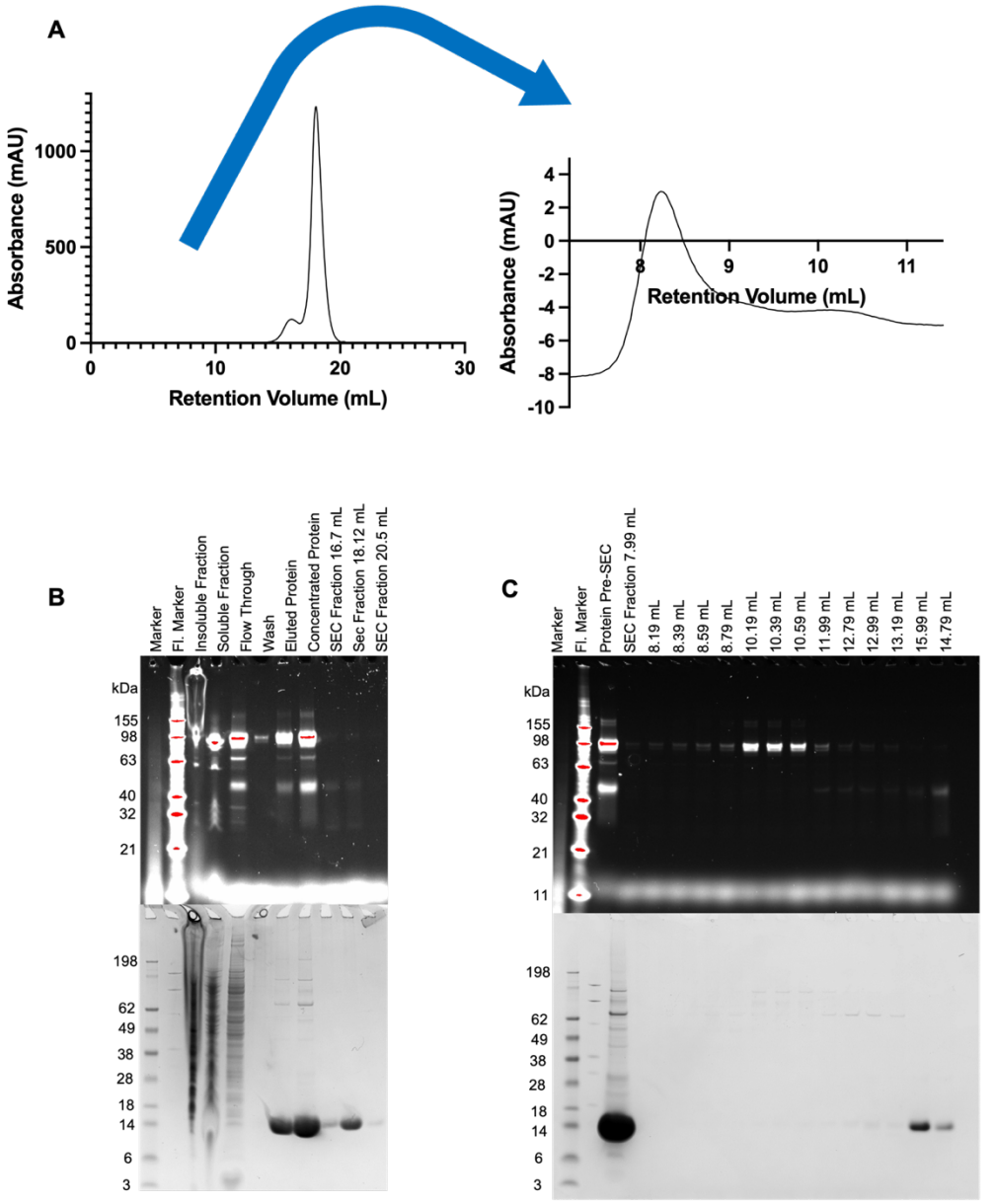

Figure 3.6 – SEC and SDS-PAGE results from the improved large-scale protein purification using sfGFP-ABCG2 co-expressed with EMMPRIN. The detergent use for the solubilization and purification of the protein was DDM. Soluble protein binding to the resin was improved by switching to overnight incubation from a 1-hour incubation. The resin and soluble protein mixture was then purified through a gravity column before further purification with SEC (**A**). Samples of the protein before SEC and selected SEC fractions were then electrophoresed through SDS-PAGE (**B** and **C**). Top image from **B** is a fluorescent image of the gel while the bottom image was taken after staining.

At first, it appeared there was a decent signal of desired purified protein that eluted at around the retention volume of 18 mL (Figure 3.6 A). However, results from the SDS-PAGE gel showed that this large peak from the SEC spectrum was not sfGFP-ABCG2 based on undetected bands at around 98 kDa in the SEC fractions (Figure 3.6 B). The large peak was most likely unbound anti-GFP nanobody that was introduced during the purification process. Further investigation determined that the sfGFP-ABCG2 protein had eluted from the SEC column when 10 – 12 mL of mobile phase had passed through. Evidence is displayed by the very small peak that can be seen in the zoomed in SEC spectrum (Figure 3.6 A) as well the detectable fluorescent bands observed in an SDS-PAGE gel (Figure 3.6 C).

Although the purified sfGFP-ABCG2 co-expressed with EMMPRIN was eventually concentrated to 0.5 mL of 7.4 mg/mL, this was not enough protein to carry out any biophysical experiments. A repeat of large-scale sfGFP-ABCG2 protein production was attempted using HEK293T suspension adapted His-sfGFP-ABCG2 cells for an even larger harvest of membrane preparations (Horsey, 2018; Mitchell-White et al., 2024). Unfortunately, time constraints and user availability at the MPL prevented another visit to the facility to re-attempt any more large-scale purifications. Yet this preliminary work has set in place the conditions required to solubilize and purify ABCG2, and the use of suspension cells has increased the yield of cells and membranes by a factor of ten. This opens the door for future biophysical investigations of ABCG2.

Chapter 4 Discussion

This project aimed to investigate how ABCG2 is regulated through protein-protein interactions in order to better understand its role in multidrug resistance (MDR). It is important to study ABCG2 protein-protein interactions so that therapeutics targeting MDR can be developed. One of the questions explored was whether ABCG2 interacts with alpha-1-acid glycoprotein (AAG), and if so, whether AAG enhances ABCG2 drug efflux. This question was inspired by previous experiments showing that albumin, a plasma protein similar to AAG, binds to ABCG2 and increases its efflux (Desuzinges-Mandon et al., 2010; Szafraniec and Fiedor, 2021). Although Park et al. (2021) did not directly study ABCG2:AAG interactions, their data suggested that such interactions may occur and influence drug pharmacokinetics. Another question investigated was whether ABCG2 interacts with extracellular matrix metalloproteinase inducer (EMMPRIN), and if so, whether co-expression with EMMPRIN increases ABCG2 expression. Zhou et al. (2013) observed elevated ABCG2 expression in the presence of EMMPRIN and hypothesized that EMMPRIN acts as a chaperone protein, stabilizing ABCG2 at the cell surface. Although this project did not detect any functional or biophysical interactions between ABCG2 and AAG or EMMPRIN, it makes way for future studies to explore these interactions further, along with other protein-protein interactions that may influence ABCG2-mediated MDR.

4.1 Summary of Results

Monolayer transport assays determined that HEK293T-sfGFP-ABCG2 cells had effluxed mitoxantrone (MX), a fluorescent ABCG2 substrate, out of cells as expected. This was observed through low intracellular MX fluorescence. In the presence of Ko143, an ABCG2 inhibitor, intracellular MX fluorescence was observed to be much higher concluding that the inhibitor significantly decreased ABCG2 efflux. However, with the addition of AAG to the transport assays, data that was collected showed that there was no increase in ABCG2 efflux of MX. When efflux rates of cells only exposed to MX were compared with cells exposed to both MX and AAG, statistical analysis determined that there was no difference. Therefore, the data collected during this thesis cannot prove that AAG impacts ABCG2 efflux.

ABCG2:EMMPRIN functional interactions were studied through densitometric analysis of western blots. Low expressing HEK293T-sfGFP-ABCG2 were co-transfected with EMMPRIN at various concentrations and then harvested over time and analysed through densitometric analysis of western blots to determine if the presence of EMMPRIN increased ABCG2 expression. Results indicated that EMMPRIN had no effect on ABCG2 expression since increased ABCG2 expression was not observed. With this data, it cannot be determined whether ABCG2 interacts with EMMPRIN.

Cell culture production of HEK293T-sfGFP-ABCG2 and co-transfection with EMMPRIN was scaled up to accommodate for large-scale

purification of sfGFP-ABCG2 constructs. It was necessary to purify the sfGFP-ABCG2 constructs if biophysical interactions with AAG or EMMPRIN were to be studied. Due to the low protein yield of the purified products, biophysical experiments were unable to be carried out. However, through the detergent screening, it was determined that DDM was the best detergent to use for purification of sfGFP-ABCG2. Furthermore, improvements to the purification were achieved.

4.2 Limitations and Alternative Ways to Investigate Hypotheses

With any experiments, there are limitations that need to be addressed as well as alternative ways to approach the hypothesis. Due to the acidic nature of AAG, it is known to transport basic and neutral lipophilic drugs such as mitoxantrone. Furthermore, AAG has been demonstrated to have a relatively high binding affinity to mitoxantrone (Finlay and Baguley, 2000). Therefore, since MX is able to bind to AAG, it can be expected that ABCG2 efflux of MX would increase if ABCG2:AAG interactions were present. However, this was not observed in the time-course transport assays. To determine the impact of albumin on ABCG2 efflux of photosensitizer drugs, Szafraniec and Fiedor (2021) also used plate-based transport assays. However, their methods differed in several ways. Firstly, they did not de-energize cells and allowed cells to accumulate the photosensitizer drugs for three hours. Secondly, fluorescence of accumulated substrates was measured by extracting them from the cells with a 1:1 (v/v) ethanol/DMSO mixture after specific efflux timepoints that spanned

from 0 to 24 hours. When accumulated mitoxantrone was measured after ABCG2 efflux for this project, fluorescence of the accumulated substrate was measured within the cell assay and not separately. Thirdly, Szafraniec and Fiedor (2021) used various albumin concentrations from 0 to 500 μM when determining its influence on ABCG2 efflux. The transport assays for this project only used the physiological concentration of AAG (5 μM) when investigating ABCG2:AAG and did not explore other concentrations.

An alternative way that functional ABCG2:AAG interactions could have been studied was through flow cytometry. Though Szafraniec and Fiedor (2021) ABCG2:albumin interactions were only measured through a plate-based transport assay, they also did perform flow cytometric experiments to study the distribution of the photosensitizer drugs among the cells after various efflux periods. Sajid et al. (2020) investigated rhodamine 123 efflux by ABCB1 using flow cytometry after cells had been de-energized. In a similar manner, AAG interactions on MX efflux by ABCG2 could be studied by flow cytometry instead of a plate-based transport assay. However, with the various efflux timepoints, this would prove difficult to carry out.

Perhaps the reason why ABCG2:AAG interactions were not observed during this project was that AAG does not physically bind to ABCG2 like albumin does. Often, functional and biophysical protein-protein interactions are linked. The goal with the purified wildtype sfGFP-ABCG2 construct was to test any binding affinity it displayed with soluble AAG (procured through Sigma-Aldrich) through flow-induced

dispersion analysis (FIDA). However, with the time constraints of this project, this was unable to be carried out. If AAG is discovered to physically not bind to ABCG2, then it is likely that it also does not interact with ABCG2 in a functional manner and does not cause increased efflux.

To investigate ABCG2:EMMPRIN, there were alternative methods that may have been explored instead. Since EMMPRIN is believed to stabilize ABCG2 at the cell surface, ideally an experiment that measured only cell-surface ABCG2 should have been implemented. With the densitometric analysis performed through western blots, this did not strictly allow for the study of changes in ABCG2 expression on the cell surface. The western blots used whole cell lysates, therefore, ABCG2 expression within and on the cell-surface was not differentiated but was measured all together. A potential method to study functional ABCG2:EMMPRIN interactions is through an image-based experiment. First, HEK293T-sfGFP-ABCG2 cells would be imaged before co-transfection with EMMPRIN. Images of co-transfected cells would then be taken over several days and analyzed for any changes in ABCG2 expression measured by sfGFP fluorescence. Data from co-transfected cells would be collected alongside cells that had not been co-transfected with EMMPRIN, and the data would be compared as appropriate. Another way to study changes in cell-surface ABCG2 expression is through flow cytometry. Cells stably transfected with ABCG2 would be incubated with a 5D3 monoclonal antibody conjugated to a fluorophore to measure cell-surface ABCG2

expression. The 5D3 antibody would be useful to use because it only interacts with the extracellular portion of ABCG2. Cell-surface ABCG2 expression levels would then be compared with stably transfected ABCG2 cells that were co-transfected with EMMPRIN for comparison through flow cytometry.

Part of the goal of this project had been to look at biophysical interactions between ABCG2 and EMMPRIN. However, before this could be tested, EMMPRIN was required to be co-expressed and then co-purified with sfGFP-ABCG2 through large-scale transfections and purification. It was required for EMMPRIN to be co-expressed with ABCG2 because EMMPRIN is also a membrane protein. Once suitable purified proteins were obtained, ABCG2:EMMPRIN biophysical interactions were planned to be tested through nano differential scanning fluorimetry (nanoDSF). NanoDSF is a method to measure protein stability and unfolding by applying a temperature gradient and measuring any changes in fluorescence emission from the protein of interest (Gao et al., 2020). Results from this technique would help determine whether EMMPRIN does stabilize ABCG2 at the plasma membrane. CD86 was also co-expressed with sfGFP-ABCG2 as a control to be used for nanoDSF for ABCG2:EMMPRIN interactions since CD86 is a membrane protein with a similar molecular weight to that of EMMPRIN. However, as mentioned with the ABCG2:AAG biophysical interaction aspect of the project, timing did not allow for this to transpire.

Although biophysical experiments were unable to be carried out, an improved purification protocol of sfGFP-ABCG2 constructs was established with expertise from the Membrane Protein Lab (MPL) at Diamond Light Source Ltd. Through this newly acquired knowledge, a pull-down assay can be performed where ABCG2 is purified and then analyzed through mass spectrometry to determine what ABCG2 protein-protein interactions can be determined. This would then allow hypotheses of ABCG2 protein-protein interactions to come from the data, and the most promising interactions could be further investigated with functional and other biophysical experiments.

4.3 Conclusion

The goal of this project was to investigate ABCG2:AAG and ABCG2:EMMPRIN interactions, and if present, how these interactions affected MDR caused by ABCG2. Although data produced from the project did not confirm any of these interactions to exist, alternative methods of studying the interactions have been suggested for future investigations. Furthermore, improved protein purification protocols of ABCG2 constructs lay the groundwork for future biophysical experiments that allow the investigation of ABCG2 protein-protein interactions. Ultimately, this will give further insight into ABCG2 regulation and help discover new therapeutics that target MDR.

Chapter 5 References

Allen, J. D., van Loevezijn, A., Lakhai, J. M., van der Valk, M., van Tellingen, O., Reid, G., Schellens, J. H. M., Koomen, G.-J., & Schinkel, A. H. (2002). Potent and Specific Inhibition of the Breast Cancer Resistance Protein Multidrug Transporter in Vitro and in Mouse Intestine by a Novel Analogue of Fumitremorgin C1. *Molecular Cancer Therapeutics*, *1*(6), 417–425.

Arkin, M. R., Tang, Y., & Wells, J. A. (2014). Small-Molecule Inhibitors of Protein-Protein Interactions: Progressing toward the Reality. *Chemistry & Biology*, *21*(9), 1102–1114. https://doi.org/10.1016/j.chembiol.2014.09.001

Bayburt, T. H., Grinkova, Y. V., & Sligar, S. G. (2002). Self-Assembly of Discoidal Phospholipid Bilayer Nanoparticles with Membrane Scaffold Proteins. *Nano Letters*, *2*(8), 853–856. https://doi.org/10.1021/nl025623k

Bayburt, T. H., & Sligar, S. G. (2010). Membrane protein assembly into Nanodiscs. *FEBS Letters*, *584*(9), 1721–1727. https://doi.org/10.1016/j.febslet.2009.10.024

Boussif, O., Lezoualc'h, F., Zanta, M. A., Mergny, M. D., Scherman, D., Demeneix, B., & Behr, J. P. (1995). A versatile vector for gene and oligonucleotide transfer into cells in culture and in vivo: Polyethylenimine. *Proceedings of the National Academy of Sciences of the United States of America*, *92*(16), 7297–7301. https://doi.org/10.1073/pnas.92.16.7297

Dean, M., & Annilo, T. (2005). Evolution of the Atp-Binding Cassette (abc) Transporter Superfamily in Vertebrates. *Annual Review of Genomics and Human Genetics*, *6*(1), 123–142. https://doi.org/10.1146/annurev.genom.6.080604.162122

Dean, M., Moitra, K., & Allikmets, R. (2022). The human ATP-binding cassette (ABC) transporter superfamily. *Human Mutation*, *43*(9), 1162–1182. https://doi.org/10.1002/humu.24418

Desuzinges-Mandon, E., Arnaud, O., Martinez, L., Huché, F., Di Pietro, A., & Falson, P. (2010). ABCG2 Transports and Transfers Heme to Albumin through Its Large Extracellular Loop. *The Journal of Biological Chemistry*, *285*(43), 33123–33133. https://doi.org/10.1074/jbc.M110.139170

Dörr, J. M., Scheidelaar, S., Koorengevel, M. C., Dominguez, J. J., Schäfer, M., van Walree, C. A., & Killian, J. A. (2016). The styrene–maleic acid copolymer: A versatile tool in membrane research. *European Biophysics Journal*, *45*(1), 3–21. https://doi.org/10.1007/s00249-015-1093-y

Doyle, L. A., & Ross, D. D. (2003). Multidrug resistance mediated by the breast cancer resistance protein BCRP (ABCG2). *Oncogene*, *22*(47), 7340–7358. https://doi.org/10.1038/sj.onc.1206938

Eckenstaler, R., & Benndorf, R. A. (2020). 3D structure of the transporter ABCG2—What's new? *British Journal of Pharmacology*, *177*(7), 1485–1496. https://doi.org/10.1111/bph.14991

Fanali, G., di Masi, A., Trezza, V., Marino, M., Fasano, M., & Ascenzi, P. (2012). Human serum albumin: From bench to bedside. *Molecular Aspects of Medicine*, *33*(3), 209–290. https://doi.org/10.1016/j.mam.2011.12.002

Finlay, G. J., & Baguley, B. C. (2000). Effects of protein binding on the in vitro activity of antitumour acridine derivatives and related anticancer drugs. *Cancer Chemotherapy and Pharmacology*, *45*(5), 417–422. https://doi.org/10.1007/s002800051011

Gao, K., Oerlemans, R., & Groves, M. R. (2020). Theory and applications of differential scanning fluorimetry in early-stage drug discovery. *Biophysical Reviews*, *12*(1), 85–104. https://doi.org/10.1007/s12551-020-00619-2

Goehring, A., Lee, C.-H., Wang, K. H., Michel, J. C., Claxton, D. P., Baconguis, I., Althoff, T., Fischer, S., Garcia, K. C., & Gouaux, E. (2014). Screening and large-scale expression of membrane proteins in mammalian cells for structural studies. *Nature Protocols*, *9*(11), 2574–2585. https://doi.org/10.1038/nprot.2014.173

Hedin, L. E., Illergård, K., & Elofsson, A. (2011). An Introduction to Membrane Proteins. *Journal of Proteome Research*, *10*(8), 3324–3331. https://doi.org/10.1021/pr200145a

Henriksen, U., Fog, J. U., Litman, T., & Gether, U. (2005). Identification of Intra- and Intermolecular Disulfide Bridges in the Multidrug Resistance Transporter ABCG2 *. *Journal of Biological Chemistry*, *280*(44), 36926–36934. https://doi.org/10.1074/jbc.M502937200

Hollenstein, K., Dawson, R. J., & Locher, K. P. (2007). Structure and mechanism of ABC transporter proteins. *Current Opinion in Structural Biology*, *17*(4), 412–418. https://doi.org/10.1016/j.sbi.2007.07.003

Horsey, A. J., Cox, M. H., Sarwat, S., & Kerr, I. D. (2016). The multidrug transporter ABCG2: Still more questions than answers. *Biochemical Society Transactions*, *44*(3), 824–830. https://doi.org/10.1042/BST20160014

Horsey, A. J. (2018). *Analysis of ABCG2 pharmacology and oligomerization by solution based fluorescence correlation spectroscopy*. PhD Thesis, University of Nottingham.

Horsey, A. J., Briggs, D. A., Holliday, N. D., Briddon, S. J., & Kerr, I. D. (2020). Application of fluorescence correlation spectroscopy to study substrate binding in styrene maleic acid lipid copolymer encapsulated ABCG2. *Biochimica et Biophysica Acta (BBA) - Biomembranes*, *1862*(6), 183218. https://doi.org/10.1016/j.bbamem.2020.183218

Ishikawa, T., Zhu, B.-L., & Maeda, H. (2006). Effect of sodium azide on the metabolic activity of cultured fetal cells. *Toxicology and Industrial Health*, *22*(8), 337–341. https://doi.org/10.1177/0748233706071737

Jackson, H. K., Mitoko, C., Linke, F., Macarthur, D., Kerr, I. D., & Coyle, B. (2023). Extracellular Vesicles Potentiate Medulloblastoma Metastasis in an EMMPRIN and MMP-2 Dependent Manner. *Cancers*, *15*(9), 2601. https://doi.org/10.3390/cancers15092601

Jackson, S. M., Manolaridis, I., Kowal, J., Zechner, M., Taylor, N. M. I., Bause, M., Bauer, S., Bartholomaeus, R., Bernhardt, G., Koenig, B., Buschauer, A., Stahlberg, H., Altmann, K.-H., & Locher, K. P. (2018). Structural basis of small-molecule inhibition of human multidrug transporter ABCG2. *Nature Structural & Molecular Biology*, *25*(4), 333–340. https://doi.org/10.1038/s41594-018-0049-1

Kage, K., Fujita, T., & Sugimoto, Y. (2005). Role of Cys-603 in dimer/oligomer formation of the breast cancer resistance protein BCRP/ABCG2. *Cancer Science*, *96*(12), 866–872. https://doi.org/10.1111/j.1349-7006.2005.00126.x

Kapoor, P., Briggs, D. A., Cox, M. H., & Kerr, I. D. (2020). Disruption of the Unique ABCG-Family NBD:NBD Interface Impacts Both Drug Transport and ATP Hydrolysis. *International Journal of Molecular Sciences*, *21*(3), Article 3. https://doi.org/10.3390/ijms21030759

Kerr, I. D., Haider, A. J., & Gelissen, I. C. (2011). The ABCG family of membrane-associated transporters: You don't have to be big to be mighty. *British Journal of Pharmacology*, *164*(7), 1767–1779. https://doi.org/10.1111/j.1476-5381.2010.01177.x

Laemmli, U. K. (1970). Cleavage of Structural Proteins during the Assembly of the Head of Bacteriophage T4. *Nature*, *227*(5259), 680–685. https://doi.org/10.1038/227680a0

Lee, J.-Y., Kinch, L. N., Borek, D. M., Wang, J., Wang, J., Urbatsch, I. L., Xie, X.-S., Grishin, N. V., Cohen, J. C., Otwinowski, Z., Hobbs, H. H., & Rosenbaum, D. M. (2016). Crystal structure of the human sterol transporter ABCG5/ABCG8. *Nature*, *533*(7604), Article 7604. https://doi.org/10.1038/nature17666

Lin, L., Yee, S. W., Kim, R. B., & Giacomini, K. M. (2015). SLC transporters as therapeutic targets: Emerging opportunities. *Nature Reviews Drug Discovery*, *14*(8), 543–560. https://doi.org/10.1038/nrd4626

Manolaridis, I., Jackson, S. M., Taylor, N. M. I., Kowal, J., Stahlberg, H., & Locher, K. P. (2018). Cryo-EM structures of a human ABCG2 mutant trapped in ATP-bound and substrate-bound states. *Nature*, *563*(7731), 426–430. https://doi.org/10.1038/s41586-018-0680-3

Mazia, D., Schatten, G., & Sale, W. (1975). Adhesion of cells to surfaces coated with polylysine. Applications to electron microscopy. *The Journal of Cell Biology*, *66*(1), 198–200.

Mitchell-White, J. I., Briggs, D. A., Mistry, S. J., Mbiwan, H. A., Kellam, B., Holliday, N. D., Briddon, S. J., & Kerr, I. D. (2024). A time-resolved Förster resonance energy transfer assay to investigate drug and inhibitor binding to ABCG2. *Archives of Biochemistry and Biophysics*, *753*, 109915. https://doi.org/10.1016/j.abb.2024.109915

Nakagawa, H., Wakabayashi-Nakao, K., Tamura, A., Toyoda, Y., Koshiba, S., & Ishikawa, T. (2009). Disruption of N-linked glycosylation enhances ubiquitin-mediated proteasomal degradation of the human ATP-binding cassette transporter ABCG2. *The FEBS Journal*, *276*(24), 7237–7252. https://doi.org/10.1111/j.1742-4658.2009.07423.x

Pajak, B., Siwiak, E., Sołtyka, M., Priebe, A., Zieliński, R., Fokt, I., Ziemniak, M., Jaśkiewicz, A., Borowski, R., Domoradzki, T., & Priebe, W. (2020). 2-Deoxy-d-Glucose and Its Analogs: From Diagnostic to Therapeutic Agents. *International Journal of Molecular Sciences*, *21*(1), Article 1. https://doi.org/10.3390/ijms21010234

Park, J.-W., Chung, H., Kim, K.-A., Kim, J.-M., Park, I.-H., Lee, S., & Park, J.-Y. (2021). ABCG2 Single Nucleotide Polymorphism Affects Imatinib Pharmacokinetics in Lower Alpha-1-Acid Glycoprotein Levels in Humans. *Frontiers in Pharmacology*, *12*, 658039. https://doi.org/10.3389/fphar.2021.658039

Sajid, A., Lusvarghi, S., Murakami, M., Chufan, E., Abel, B., Gottesman, M., Durell, S., & Ambudkar, S. (2020). Reversing the direction of drug transport mediated by the human multidrug transporter P-glycoprotein. *Proceedings of the National Academy of Sciences*, *117*(47), 29609-29617. https://doi.org/10.1073/pnas.2016270117

Sajid, A., Rahman, H., & Ambudkar, S. V. (2023). Advances in the structure, mechanism and targeting of chemoresistance-linked ABC transporters. *Nature Reviews Cancer*, 1–18. https://doi.org/10.1038/s41568-023-00612-3

Sarkadi, B., Homolya, L., Szakács, G., & Váradi, A. (2006). Human Multidrug Resistance ABCB and ABCG Transporters: Participation in a Chemoimmunity Defense System. *Physiological Reviews*, *86*(4), 1179–1236. https://doi.org/10.1152/physrev.00037.2005

Shi, J., Pabon, K., Ding, R., & Scotto, K. W. (2024). ABCG2 and SLC1A5 functionally interact to rewire metabolism and confer a survival advantage to cancer cells under oxidative stress. *Journal of Biological Chemistry*, *300*(6). https://doi.org/10.1016/j.jbc.2024.107299

Szafraniec, M. J., & Fiedor, L. (2021). One ring is not enough to rule them all. Albumin-dependent ABCG2-mediated transport of chlorophyll-derived photosensitizers. *European Journal of Pharmaceutical Sciences*, *167*, 106001. https://doi.org/10.1016/j.ejps.2021.106001

Szklarczyk, D., Kirsch, R., Koutrouli, M., Nastou, K., Mehryary, F., Hachilif, R., Gable, A. L., Fang, T., Doncheva, N. T., Pyysalo, S., Bork, P., Jensen, L. J., & von Mering, C. (2023). The STRING database in 2023: Protein–protein association networks and functional enrichment analyses for any sequenced

genome of interest. *Nucleic Acids Research*, *51*(D1), D638–D646. https://doi.org/10.1093/nar/gkac1000

Taylor, N. M. I., Manolaridis, I., Jackson, S. M., Kowal, J., Stahlberg, H., & Locher, K. P. (2017). Structure of the human multidrug transporter ABCG2. *Nature*, *546*(7659), 504–509. https://doi.org/10.1038/nature22345

Theodoulou, F. L., & Kerr, I. D. (2015). ABC transporter research: Going strong 40 years on. *Biochemical Society Transactions*, *43*(5), 1033–1040. https://doi.org/10.1042/BST20150139

Towbin, H., Staehelin, T., & Gordon, J. (1979). Electrophoretic transfer of proteins from polyacrylamide gels to nitrocellulose sheets: Procedure and some applications. *Proceedings of the National Academy of Sciences*, *76*(9), 4350–4354. https://doi.org/10.1073/pnas.76.9.4350

van Herwaarden, A. E., & Schinkel, A. H. (2006). The function of breast cancer resistance protein in epithelial barriers, stem cells and milk secretion of drugs and xenotoxins. *Trends in Pharmacological Sciences*, *27*(1), 10–16. https://doi.org/10.1016/j.tips.2005.11.007

van Herwaarden, A. E., Wagenaar, E., Merino, G., Jonker, J. W., Rosing, H., Beijnen, J. H., & Schinkel, A. H. (2007). Multidrug Transporter ABCG2/Breast Cancer Resistance Protein Secretes Riboflavin (Vitamin B2) into Milk. *Molecular and Cellular Biology*, *27*(4), 1247–1253. https://doi.org/10.1128/MCB.01621-06

Wakabayashi, K., Nakagawa, H., Adachi, T., Kii, I., Kobatake, E., Kudo, A., & Ishikawa, T. (2006). Identification of cysteine residues critically involved in homodimer formation and protein expression of human ATP-binding cassette transporter ABCG2: A new approach using the flp recombinase system. *Journal of Experimental Therapeutics & Oncology*, *5*(3), 205–222.

Wong, K. (2015). *Dynamics and oligomerisation of ABCG2 investigated using various fluorescence techniques.* PhD Thesis, University of Nottingham.

Wong, K., Briddon, S. J., Holliday, N. D., & Kerr, I. D. (2016). Plasma membrane dynamics and tetrameric organisation of ABCG2 transporters in mammalian cells revealed by single particle imaging techniques. *Biochimica et Biophysica Acta (BBA) - Molecular Cell Research*, *1863*(1), 19–29. https://doi.org/10.1016/j.bbamcr.2015.10.002

Xie, Y., Xu, K., Linn, D. E., Yang, X., Guo, Z., Shimelis, H., Nakanishi, T., Ross, D. D., Chen, H., Fazli, L., Gleave, M. E., & Qiu, Y. (2008). The 44-kDa Pim-1 Kinase Phosphorylates BCRP/ABCG2 and Thereby Promotes Its Multimerization and Drug-resistant Activity in Human Prostate Cancer Cells. *Journal of Biological Chemistry*, *283*(6), 3349–3356. https://doi.org/10.1074/jbc.M707773200

Xu, J., Xiong, G., Cao, Z., Huang, H., Wang, T., You, L., Zhou, L., Zheng, L., Hu, Y., Zhang, T., & Zhao, Y. (2016). PIM-1 contributes to the malignancy of pancreatic

cancer and displays diagnostic and prognostic value. *Journal of Experimental & Clinical Cancer Research*, *35*(1), 133. https://doi.org/10.1186/s13046-016-0406-z

Zhou, S., Liao, L., Chen, C., Zeng, W., Liu, S., Su, J., Zhao, S., Chen, M., Kuang, Y., Chen, X., & Li, J. (2013). CD147 mediates chemoresistance in breast cancer via ABCG2 by affecting its cellular localization and dimerization. *Cancer Letters*, *337*(2), 285–292. https://doi.org/10.1016/j.canlet.2013.04.025